Geological Validation of Airborne Geophysical Anomalies for Lithium-Pegmatite Exploration, Northern Portugal

Alane Iasmin Cordara da Silva
Master in Geology
Department of Geosciences, Environment, and Spatial Planning
Faculty of Sciences of the University of Porto
2025

U.PORTO
FACULDADE DE CIÊNCIAS
UNIVERSIDADE DO PORTO

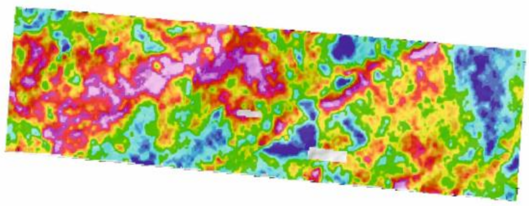

Geological Validation of Airborne Geophysical Anomalies for Lithium-Pegmatite Exploration, Northern Portugal

Alane Iasmin Cordara da Silva

Dissertation carried out as part of the Master in Geology
Department of Geosciences, Environment, and Spatial Planning
2025

U.PORTO
FC FACULDADE DE CIÊNCIAS UNIVERSIDADE DO PORTO

Supervisor
Alexandre Martins Campos de Lima, Associate Professor, Faculty of Sciences of the University of Porto

Co-supervisor
Rui Miguel Marques Moura, Associate Professor, University of Aveiro

"Èṣù matou um pássaro ontem,

com uma pedra que só jogou hoje."

LARÓYÈ!

Acknowledgements

I thank myself, for having dared to leave, leaving behind what I love most in search of who I am.

To my Guias and Orixás, who gave me solid ground when I took the leap.

To my parents, for being everything and above all, home. Thank you for never letting me forget that I will always have a place to return to.

To Professor Alexandre Lima and researcher Ana Carvalho, whose guidance, support, and trust were fundamental to the completion of this dissertation.

To João, for the care, the patience, and for giving me the gift of a peaceful love.

And to all the people who, in one way or another, contributed to my path, on the trails of geology or the roads of life, I leave here my deepest and most sincere gratitude.

Resumo

Os pegmatitos litiníferos tornaram-se alvos críticos de prospeção no contexto da transição energética e da crescente procura por metais estratégicos. No Campo Aplito-Pegmatítico de Barroso-Alvão (Norte de Portugal), os esforços de exploração são, por vezes, dificultados pela limitada exposição superficial dos corpos pegmatíticos, pelo seu avançado grau de alteração e pela complexidade geológica na rocha encaixante. Esta dissertação explora a aplicação da espectrometria de raios gama aérea, especificamente a interpretação de anomalias na concentração de tório (Th), como método geofísico para a identificação de ocorrências de pegmatitos, sendo alguns litiníferos. Os dados radiométricos do projeto GREENPEG foram integrados com campanhas de validação de campo focadas em zonas caracterizadas por anomalias negativas de Th.

Em dez alvos principais e seis pontos fora de alvo, foram mapeados e caracterizados um total de 127 afloramentos. Corpos pegmatíticos foram frequentemente confirmados em áreas com anomalias negativas de Th, sustentando a hipótese de que pegmatitos, tipicamente empobrecidos em Th, podem ser eficazmente delimitados com base em assinaturas radiométricas. As observações de campo também revelaram um forte controlo estrutural na intrusão dos pegmatitos, particularmente ao longo de estruturas relacionadas com a fase D_3. Além disso, as rochas metassedimentares encaixantes apresentaram veios de quartzo abundantes, especialmente a leste do rio Tâmega, o que pode influenciar o sinal radiométrico devido ao maior teor de sílica e à possível sobreposição de anomalias geofísicas.

A correlação entre os dados geofísicos e os afloramentos de pegmatito mapeados confirma a eficácia deste método neste contexto geológico. Adicionalmente, o estudo sugere que as anomalias positivas de Th também merecem investigação complementar, uma vez que podem ocultar ou ser influenciadas por complexidades litológicas ou estruturais. Os novos corpos pegmatíticos identificados durante o trabalho de campo devem ser alvo de análises mineralógicas e geoquímicas mais aprofundadas para avaliar o seu potencial de mineralização em lítio. De forma geral, este trabalho destaca a importância de integrar dados geofísicos remotos com validação geológica direcionada em campo em províncias pegmatíticas.

Palavras-chave: Pegmatitos, Espectrometria de Raios Gama, Tório, Prospeção Mineral

Abstract

Lithium-bearing pegmatites have become critical exploration targets in the context of the energy transition and the growing demand for strategic metals. In the Barroso-Alvão Aplite-Pegmatite Field (Northern Portugal), exploration efforts are often hindered by the limited surface exposure of pegmatite bodies, their advanced degree of weathering, and the geological complexity of the host rocks. This dissertation explores the application of airborne gamma-ray spectrometry, specifically the interpretation of thorium (Th) concentration anomalies, as a geophysical method for the identification of pegmatite occurrences, including lithium-bearing ones. Radiometric data from the GREENPEG project were integrated with field validation campaigns focused on areas characterized by negative Th anomalies.

Across ten main targets and six off-target sites, a total of 127 outcrop points were mapped and characterized. Pegmatite bodies were frequently confirmed in areas of negative Th anomalies, typically depleted in Th, can be effectively delineated through radiometric signatures. Field observations also revealed a strong structural control on pegmatite emplacement, particularly along D_3-related features. Furthermore, the metasedimentary host rocks commonly displayed abundant quartz veining, particularly east of the Tâmega River, which may influence the radiometric signal due to enhanced silica content and potential overprinting of anomalies.

The correlation between geophysical data and mapped pegmatite outcrops confirms the efficacy of this method in this geological setting. Additionally, the study suggests that positive Th anomalies may also merit further investigation, as they may conceal or be influenced by lithological or structural complexities. Newly discovered pegmatitic bodies identified during fieldwork should be subjected to further mineralogical and geochemical analysis to assess their potential for lithium mineralization. Overall, this work highlights the importance of integrating remote geophysical data with targeted geological field validation in pegmatite provinces.

Keywords: Pegmatites, Gamma-ray Spectrometry, Thorium, Mineral Exploration

Table of Contents

List of Tables

List of Figures

List of Abbreviations

FCUP	FACULTY OF SCIENCES OF THE UNIVERSITY OF PORTO
UP	UNIVERSITY OF PORTO
PPM	PARTS PER MILLION
Th	THORIUM
D_1	FIRST PHASE OF DEFORMATION OF VARISCAN OROGENY
D_2	SECOND PHASE OF DEFORMATION OF VARISCAN OROGENY
D_3	THIRD PHASE OF DEFORMATION OF VARISCAN OROGENY
S_1	MAIN FOLIATION RESULTING FROM D1
S_2	MAIN FOLIATION RESULTING FROM D2
S_3	MAIN FOLIATION RESULTING FROM D3
F_2	SECOND FAMILY OF PEGMATITIC DYKES BY LIMA (2000)
F_3	THIRD FAMILY OF PEGMATITIC DYKES BY LIMA (2000)
CIZ	CENTRAL IBERIAN ZONE
GTMZ	GALICIA TRÁS-OS-MONTES ZONE
CSD	CARRAZEDO STRUCTURAL DOMAIN
TMSD	TRÊS MINAS STRUCTURAL DOMAIN
LCT	LITHIUM (L), CESIUM (C) AND TANTALUM (T)
NYF	NIOBIUM (N), YTTRIUM (Y) AND FLUORINE (F)
PG	PEGMATITE
APL	APLITIC
MTS	METASEDIMENTARY
QTZ	QUARTZ
KFS	K-FELDSPAR
SPD	SPODUMENE
MN	MANGANESE

Chapter I

Introduction

1.1 Introduction

Granitic pegmatites, particularly those enriched in lithium and other incompatible elements, have become increasingly important in the context of critical raw material supply chains and the ongoing global shift towards low-carbon energy technologies. These rocks, often formed during the late stages of magmatic differentiation or through partial melting of metasedimentary sequences, represent key targets for the extraction of lithium, cesium, tantalum, and other rare elements vital to produce batteries, electronics, and other strategic applications. Their geological complexity, however, poses significant challenges to exploration, particularly due to their variable morphology, limited surface exposure, and advanced weathering.

In regions like the Barroso-Alvão Aplite-Pegmatite Field in northern Portugal, pegmatitic bodies are typically hosted in deformed metasedimentary sequences of the Galicia-Trás-os-Montes Zone, often emplaced along structural weaknesses related to Variscan deformation phases. The tectono-metamorphic evolution of these terrains, marked by multiple deformation events and associated granite intrusions, provides a favorable setting for the generation and emplacement of LCT-type pegmatites. These bodies are frequently zoned and display mineralogical and structural features that reflect both magmatic processes and post-emplacement deformation, further complicating their detection and classification.

Given this complexity, geophysical methods have become indispensable tools in modern mineral exploration, offering indirect yet powerful means to delineate subsurface features. Among them, gamma-ray spectrometry stands out for its capacity to map the distribution of naturally occurring radioactive elements such as potassium (K), uranium (U), and thorium (Th) in the Earth's uppermost layers. As thorium tends to be incorporated early into accessory minerals during magma evolution, pegmatitic melts, particularly those of the LCT-type, are often depleted in Th relative to their host rocks. This compositional contrast makes them potential sources of negative anomalies in airborne radiometric surveys.

In this broader framework, the integration of airborne radiometric data with field validation in structurally complex domains offers a promising approach for improving the efficiency and accuracy of pegmatite exploration efforts. The present study is embedded in this methodological context, exploring the potential of gamma-ray spectrometry as a tool for identifying lithium-bearing pegmatite occurrences in northern Portugal.

1.2 Thesis Objectives

The main objective of this thesis is to evaluate the applicability and reliability of radiometric geophysical data, particularly thorium (Th) concentration anomalies, for the identification of lithium-bearing pegmatite bodies. The study is based on airborne radiometric data provided by the GREENPEG project and focuses on the interpretation of negative thorium anomalies as potential indicators of pegmatite occurrences. To validate this geophysical method, targeted fieldwork was carried out in selected anomalous zones, involving macroscopic observation and characterization of pegmatite outcrops. This included the assessment of structural features, mineral assemblages, and the spatial alignment of pegmatitic bodies in relation to the host metasedimentary rocks.

The field analysis also aimed to compare the observed geological and structural features with existing tectono-structural models of the region and with previously published studies on the geology and pegmatite systems of the Barroso-Alvão Aplite-Pegmatite Field. By integrating geophysical interpretation with direct geological evidence, the thesis seeks to determine the effectiveness of using thorium anomalies as a tool for guiding exploration in lithium-rich pegmatitic provinces and to contribute to refining exploration methodologies in similar geological contexts.

1.3 Geographical Setting

The study area (Fig. 1.1) covers approximately 25 km² and is located about 120 km northeast of the municipality of Porto, in northern Portugal. It is situated within the district of Vila Real and extends across three municipalities: Boticas, Ribeira de Pena, and Vila Pouca de Aguiar. This region is part of the Barroso-Alvão aplite-pegmatite field, which is known for its abundant lithium-bearing pegmatites and complex geological framework.

The area is traversed by the Tâmega River, which follows a predominant northeast-southwest (NE-SW) orientation, and is flanked by prominent mountain ranges, including the Serra do Alvão, Serra da Padrela, and Serra do Leiranco. These mountainous features contribute to the rugged topography and influence local drainage patterns, structural controls, and the exposure of lithological units. The combination of geological diversity and structural complexity makes this area particularly significant for the study of pegmatitic systems and associated mineralizations.

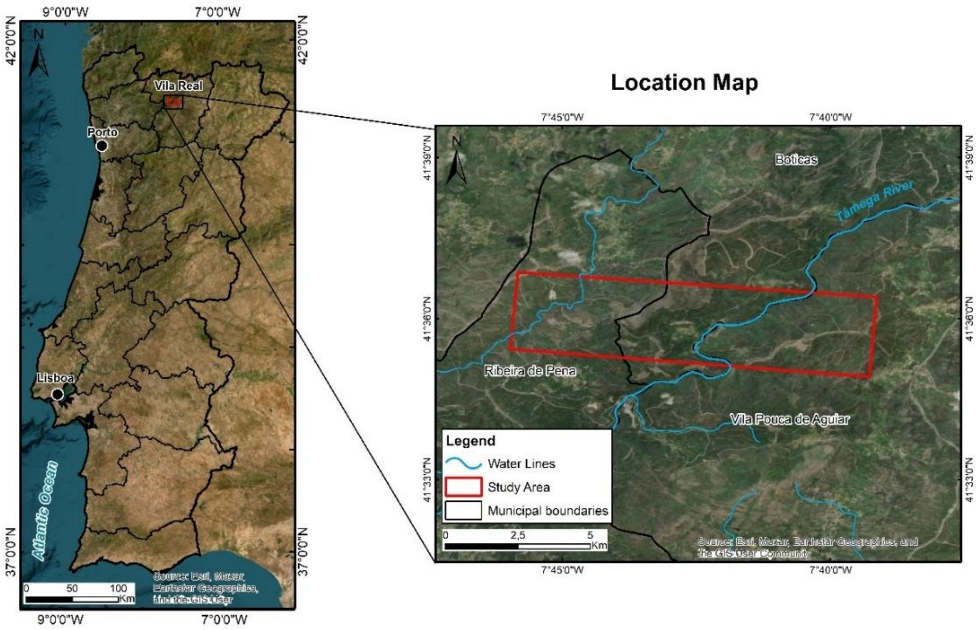

Fig. 1.1: Location map of the study area.

1.4 Thesis Structure

This thesis is structured in different chapters:

- Chapter 1 – introduces the context of the study, presents the main objectives of the thesis, and describes the geographical setting of the study area.
- Chapter 2 – details the geophysical method used in this research, with a focus on airborne Gamma-ray Spectrometry and its application to mineral exploration.
- Chapter 3 – provides a comprehensive overview of pegmatites, including their definition, genesis, classification, zoning, and spatial distribution in the European context.
- Chapter 4 – presents the geological setting of the study area, describing its geotectonic framework, deformation history, metamorphism, and main lithologies such as metasedimentary and granitic rocks.
- Chapter 5 – outlines the fieldwork methodology and presents the results of the geological validation campaigns, including mapped outcrops for each of the ten main targets and additional off-target sites.
- Chapter 6 – contains the final considerations of the study, summarizing the key findings and offering reflections on the methodology and future research directions.

Chapter II

Geophysical Methods

2.1 Introduction

The Earth's surface is composed of different types of rocks, each with specific physical properties. Thus, each lithotype exhibits characteristics. In this context, geophysical investigation conducted on the surface and subsurface provides important data about the Earth's composition and internal structure. The measurements obtained are influenced by the distribution of physical properties within the planet, which vary both vertically and laterally.

Various geophysical methods are available, each sensitive to a specific physical property (Table 2.1). However, due to the inherent ambiguity and uncertainties of these methods, it is necessary to apply processing and corrections to reduce such effects.

Table 2.1: Relationship between the physical properties of rocks and the main geophysical methods used for their investigation. Source: Adapted from Telford et al. (1990).

Physical Property	Geophysical Method
Density	Gravimetry
Magnetic Susceptibility	Magnetometry
Electrical Conductivity	Electrical or Electromagnetic Methods
Radioactivity	Radiometry
Elasticity	Seismic Methods
Thermal Conductivity	Thermometry
Luminescence	Luminescence Method

With technological advances in recent decades, geophysical methods have evolved from being secondary tools for qualitative analysis to primary sources for identifying and interpreting new mineral deposits. This evolution has been driven by the increasing scarcity of mineral resources at the surface, which has demanded exploration at greater depths and resulted in higher extraction costs. In this scenario, as highlighted by Ribeiro et al. (2013), geophysics stands out as the most cost-effective tool to identify areas with mineral potential, as well as to reveal geological structures that may host economically significant mineralizations, supporting geological and structural mapping.

Given the above, the following section presents the gamma-ray spectrometry method, which is applied in the mineral exploration of pegmatites.

2.2 Gamma-ray Spectrometry

The instability of radioactive atomic nuclei under natural conditions causes the spontaneous release of energy from their nuclear decay. The radiation emitted during this decay can occur in the form of charged alpha (α) and/or beta (β) particles, or as gamma (γ), radiation, which has low penetrating power in different materials. Alpha and beta emissions cause matter to enter an excited state, and the excess energy is released in the form of gamma radiation (IAEA, 2003 in Dantas, 2023). These emissions cause: Emission α → Ejection of 2 protons and 2 neutrons; Emission β → Ejection of a high-velocity electron or positron; Emission γ → Very short-wavelength electromagnetic radiation.

Although there are more than fifty radioactive isotopes in nature, most are extremely rare or emit low-intensity radiation. For this reason, the main sources of gamma radiation used in this method are potassium (^{40}K) and elements from the uranium (^{238}U) and thorium (^{232}Th) decay series. These elements have relatively high concentrations in the upper crust, making them essential for mineral exploration using gamma-ray spectrometry (Telford et al., 1990) (Fig. 2.3).

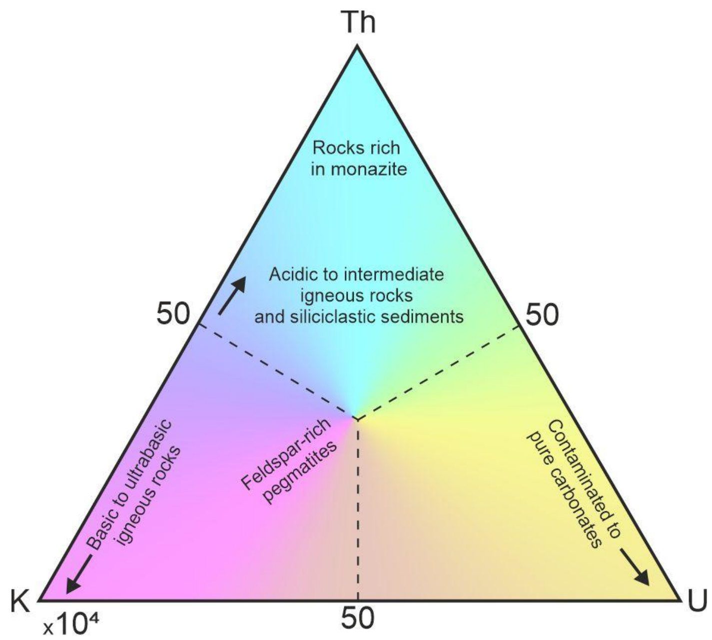

Fig. 2.1: Ternary diagram showing the relative abundance of radioactive elements in different rock types. Source: Adapted from Kearey et al. (2009).

The conversion of counts per second into concentrations of K (potassium, in %), eU (equivalent uranium, in ppm), and eTh (equivalent thorium, in ppm) provides valuable information for various applications. This transformation helps, for example, in the identification of areas affected by hydrothermal alterations, as well as enabling the analysis of their relationships with mineralizing processes in different geological contexts (Dickson & Scott, 1997 in Froede, 2017).

Initially developed to support regional geological mapping and uranium mineral exploration, gamma-ray spectrometry has undergone significant advancements in recent years (Ribeiro et al., 2013). This geophysical method works by measuring the contrast between the main sources of gamma radiation detected on the Earth's surface, with data collected using an airborne spectrometer (Fig. 2.4).

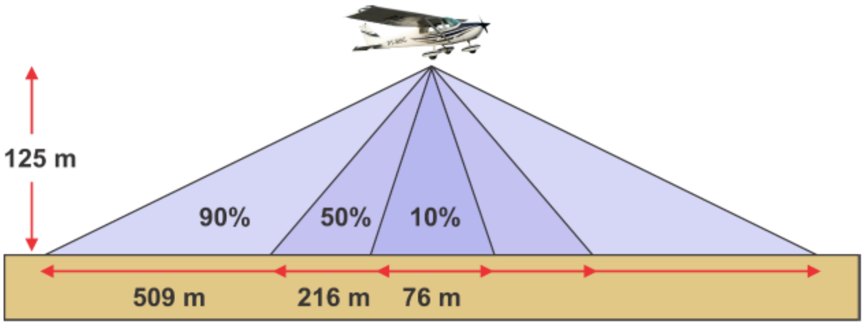

Fig. 2.2: Field of view of an airborne gamma-ray spectrometer. This figure shows, for a uniform space, the size of the area on the ground from which the gamma photons recorded by the detector originate. Source: Grasty et al. (1991b) in Dantas (2023).

The gamma-ray spectrometric method has a limited depth of penetration, reaching a maximum of about 30 to 40 cm in anhydrous environments. This low penetration is due to the interference that the medium provides to the measurements, thus reducing the average thickness investigated (Minty, 1988).

From the individual counts of the radioelements, radiometric ratio maps are created, such as U/Th, U/K, and Th/K. These maps can be used to identify changes in rock type, hydrothermal alterations, geomorphological features, and variations in the concentration of radioelements in igneous bodies. Rock types in the same region may show distinctions in the concentration of U, Th, and K, and their ratios can indicate the limits of these concentrations (Ribeiro et al., 2013).

Understanding and defining the geological contexts in which radioactive chemical elements are present is essential. For such analysis to be meaningful, it is necessary to establish geological background values. The distribution of these elements in the Earth's crust is highly heterogeneous and depends largely on the type of soil or rock. Table 2.2 presents average concentration values for various rock types (Schön, 2015).

Table 2.2: Average concentrations of K, U, and Th in various rock types. Source: Adapted from Schön, 2015.

Lithology	K (%)	U (ppm)	Th (ppm)
Continental Crust Average[a]	2,8	2,8	10,7
Granite	4,11	4,35	15,2
Gabbro	0,52	0,87	2,77
Granodiorite	2,3	2,1	8,3
Basalt	0,61	0,99	4,6
Quartzite	0,9	0,6	1,8
Limestone	0.0-2.0	2.5-2.8	0.1-7
Sandstone	1,1	0,5	1,7
Schist	2,7	3,7	12
Black Schist	2,6	20,2	10,9

(a) Rudnick & Gao, 2014

Igneous bodies can be mapped based on radioelement concentrations, as the enrichment of these elements occurs during processes such as magmatic differentiation and hydrothermal alteration. In general, more evolved igneous bodies have higher concentrations of K relative to Th and U, while less evolved ones have high values of U, Th, and K (Table 2.3). The U/K and Th/K ratios tend to be more representative than U/Th, since the geochemical behaviour of the elements is not uniform during the formation and evolution of granitic bodies (Iza et al., 2018).

Table 2.3: Radioactive minerals and their respective occurrences. Source: Kearey, Brooks, and Hill (2009).

<table>
<tr><th>Element</th><th>Mineral</th><th>Occurrence</th></tr>
<tr><td rowspan="4">Potassium</td><td>Feldspar, Orthoclase, and Microcline</td><td rowspan="2">Main constituents of acidic igneous rocks and pegmatites</td></tr>
<tr><td>Muscovite</td></tr>
<tr><td>Alunite</td><td>Alteration in volcanic rocks</td></tr>
<tr><td>Sylvite, Carnallite</td><td>Saline deposits in sediments</td></tr>
<tr><td rowspan="3">Thorium</td><td>Monazite</td><td>Granites, pegmatites and gneisses</td></tr>
<tr><td>Thorianite</td><td rowspan="2">Granites, pegmatites and placers</td></tr>
<tr><td>Thorite, Uranothorite</td></tr>
<tr><td rowspan="3">Uranium</td><td>Uraninite</td><td>Granites, pegmatites and veins of Ag, Pb, Cu, etc.</td></tr>
<tr><td>Carnotite</td><td>Sandstones</td></tr>
<tr><td>Gummitte</td><td>Associated with uraninite</td></tr>
</table>

In the case of sedimentary rocks, they generally reflect the radioelement content originating from the source rock. It is noted that in immature sediments derived from granitic rocks, an increase in their content can be expected, while in immature sediments rich in quartz, low values can be expected. The available data for metamorphic rocks suggest that, depending on which protolith the rock originated from, metamorphism does not affect the radioelement content. In general, radioactivity in sedimentary and metamorphosed sedimentary rocks is higher than in igneous rocks and other types of metamorphic rocks, except for potassium-rich granites (Telford et al. 1990).

Primary uranium can be found in oxide and silicate minerals, while uranium originating from weathering processes tends to concentrate in authigenic iron oxides and clay minerals. The main uranium minerals and occurrences include: uraninite, found in granites, pegmatites, and hydrothermal veins; carnotite, which can occur in sandstones; gummite, an alteration product of uraninite; carbonaceous black shales; and carbonate sedimentary rocks (Telford et al. 1990).

Monazite and zircon are the main thorium minerals, found in granite, gneisses, and pegmatites; thorianite, thorite, and urano thorite are present in granite, gneisses, and placers. Thorium is released by the breakdown of minerals during the weathering process and can concentrate in hydrated or oxidized, iron- or titanium-based minerals, and in clay minerals (Telford et al. 1990).

Regional airborne gamma-ray spectrometric surveys are effective tools for identifying granite intrusions and stocks through the analysis of K-Th-U spectrometer data, allowing the detection, for example, of the possible heat source of the mineralization system (Cook et al., 1996; Schetselaar; Chung; Kim, 2000 in Froede, 2017).

It is important to note that airborne gamma-ray spectrometric and magnetic surveys are generally conducted simultaneously, and although LCT pegmatites often do not contain magnetic or conductive sulphide minerals (Černý, 1982), magnetic surveys are useful for understanding the structural control on the emplacement of granites. This is because they allow for the correlation of known mineral and geochemical anomalies with regional shearing, faults, and extensional zones, which helps in identifying fluid migration pathways and potential traps for mineralization.

One of the modern applications of gamma-ray spectrometry is the possibility of identifying areas of hydrothermal alteration and establishing their relationship with base metal (Cu-Pb-Zn) mineralization processes (Shives et al., 2000). In addition, this method also contributes to the identification of possible mineralization zones in pegmatite bodies.

Chapter III

Pegmatites

3.1 Introduction

Granitic pegmatites, simply referred as pegmatites, are igneous rocks with extremely coarse grains (typically >3 cm) and granitic or nearly granitic composition. They form during the final stages of magma crystallization, when residual melts rich in volatiles and incompatible elements concentrate and segregate (Černý, 1991a; London, 2008). Pegmatites are geologically significant not only for their unique textures and internal zoning, but also for their potential to host economically important concentrations of rare metals such as lithium (Li), cesium (Cs), tantalum (Ta), niobium (Nb), yttrium (Y), and rare earth elements (REEs).

According to the most widely accepted petrogenetic models, pegmatitic melts may originate either from magmatic fractionation of parental granitic plutons or from anatexis, a process involving low-degree partial melting of pre-existing rocks (Simmons, 2007; Simmons & Webber, 2008).

Modern classification systems distinguish two major geochemical families based on mineralogical composition and geochemical signatures: the LCT-type (Li-Cs-Ta) and the NYF-type (Nb-Y-F) pegmatites (Černý, 1991a; Wise et al., 2022). While Černý's system is based on pressure-temperature conditions and chemical composition, Wise et al. emphasize mineralogical composition as the primary criterion. Together, these frameworks highlight the key measurable parameters making them essential for understanding the origin and evolution of pegmatitic melts.

Due to their enrichment in high-tech and critical elements, pegmatites have become increasingly more important targets in mineral exploration, especially in the context of the global energy transition and the growing demand for lithium-bearing minerals (Bradley et al., 2017; Müller et al., 2025).

3.2 Definition of Pegmatite

The term pegmatite was first used by Brogniart in 1813 to describe igneous rocks with intergrowths of quartz and perthitic microcline (K-feldspar). Granites with this texture were called graphic granites. Later, in 1845, Haidinger expanded the meaning of pegmatite to include very coarse-grained granitic segregations and dykes, even when graphic granite was absent (London, 2008).

Today, in the strict sense, pegmatite is a textural term used to describe intrusive igneous rocks with coarse to very coarse grains (Černý et al., 2003; Simmons, 2007; Simmons & Webber, 2008).

A more complete and widely accepted definition was proposed by London (2008, 2018). According to him, pegmatites are essentially igneous rocks, mostly granitic in composition, formed from silica-rich magmas enriched in volatiles (such as B, Li, F, P, CO_2, and H_2O) and rare elements (such as Be, Cs, Ga, Nb, Ta, Ti, Y, and REE).

They are distinguished from other igneous rocks by their complex texture, characterized by very coarse and heterogenous grain size, mineralogical zoning, and an extensive textural variety, which may include graphic texture, directional, radial, and/or skeletal growth texture of their constituent minerals.

3.3 Genesis

The most currently accepted petrogenetic models for the origin of pegmatites consist of i) magmatic fractionation of parental granitic plutons, or ii) anatexis, a process of low-grade partial melting of pre-existing rocks (Simmons, 2007; Simmons & Webber, 2008).

During the early crystallization stages of parental granitic plutons, minerals such as K-feldspar, Na-plagioclase, quartz, and muscovite ± biotite dominate. These minerals incorporate major elements like Si, Al, K, Na, and O. However, elements with very large or very small ionic radii and/or unusual charges (e.g., Cs^+, Rb^+, Sr^{2+}, Ta^{5+}, Nb^{5+}, P^{5+}, Th4+, Ti^{4+}, REE^{3+}, Li^+, Be^{2+}, B^{3+}) are poorly accommodated in these crystal structures. Such elements are considered incompatible and tend to remain concentrated in the residual melt throughout fractional crystallization. Water and other volatile components (e.g., B, F, Li, CO_2) behave similarly, becoming progressively enriched in the residual melt (Simmons, 2007; Simmons et al., 2003).

In the anatexis model, pegmatites form from the crystallization of melts generated by low-degree partial melting of pre-existing rocks. Marine metasedimentary sequences with evaporitic layers are the main protoliths, supplying both incompatible elements (e.g., Be, Ba, Cs, Nb, Rb, REE) and volatiles (e.g., B, F, Li, H_2O, CO_2) required for pegmatite formation (Simmons & Webber, 2008).

Low-degree melting of these rocks releases incompatible elements and volatiles, mostly hosted in micas such as muscovite, paragonite, phengite, and biotite-into the melt

(Černý et al., 2012). Due to the low concentration of fluxing agents (Na, Li), melting usually stops at an early stage, directly producing pegmatitic melts (Simmons, 2007; Simmons et al., 1995).

The heat source is often related to adjacent granitic intrusions, though these do not need to be comagmatic with the pegmatites (Barros, 2017).

According to Wise et al. (2022), every pegmatite should be classified into one of the defined mineral-chemical groups based on its mineralogy, which reflects the melt source. Geological context and nearby pegmatites with similar features should also be considered, as they tend to occur in clusters with consistent characteristics.

Wise et al. (2022) introduced a modern classification based on two key factors: The melt origin, whether it's a direct product of anatexis (DPA) or a residual melt from granitic magmatism (RMG) and the chemical enrichment pattern, either LCT (Group 1) or NYF (Group 2). This results in four main pegmatite types: DPA-LCT, RMG-LCT, DPA-NYF, RMG-NYF. RMG pegmatites crystallize from the highly evolved residual melts during the final stages of large granite body solidification. In contrast, DPA pegmatites form from partial melting of igneous, metaigneous, or metasedimentary rocks, often followed by magma evolution that concentrates rare elements (Fig. 3.1).

The distribution of DPA pegmatites is mainly controlled by pathway structures, which act as permeable zones concentrating and channeling melts and fluids until they reach the pegmatite formation zone (Fig. 3.2). Because volatile-rich melts have relatively low viscosity, they can infiltrate surrounding rocks along bedding or metamorphic foliation, forming sills, or they may move through ductile and brittle structures to create dykes or segregations. These pathways often predate magmatism and mineralization (Hagemann et al., 2016 in Müller et al., 2025) but may be reactivated as dilatant zones during pegmatite emplacement. Enhanced permeability can develop at multiple scales, from microcracks and grain-boundary dilation to large fractures. In RMG pegmatite fields, pathways may include preexisting faults or faults formed during granite and pegmatite emplacement (Fig. 3.3).

Structural traps are the sites where pegmatitic melts accumulate and crystallize, provided that chemical and physical conditions are favorable. These traps are usually dilatational, located in open or low-pressure segments of faults and shear zones, fold hinges, areas between rotating rigid blocks, or between rocks of contrasting rheology. First-order trapping corridors may reach regional scales. The triggers for crystallization remain uncertain but are likely related to undercooling, or possibly to the release of magmatic-hydrothermal fluids.

Once emplaced, pegmatites in the process of crystallizing (or already crystallized) can be modified by autometasomatism. Processes such as albitization or quartz-muscovite greisenization may replace spodumene, thereby reducing the Li ore grade. Most pegmatites are either late- to post-tectonic relative to regional orogenic events, or they are emplaced under anorogenic conditions.

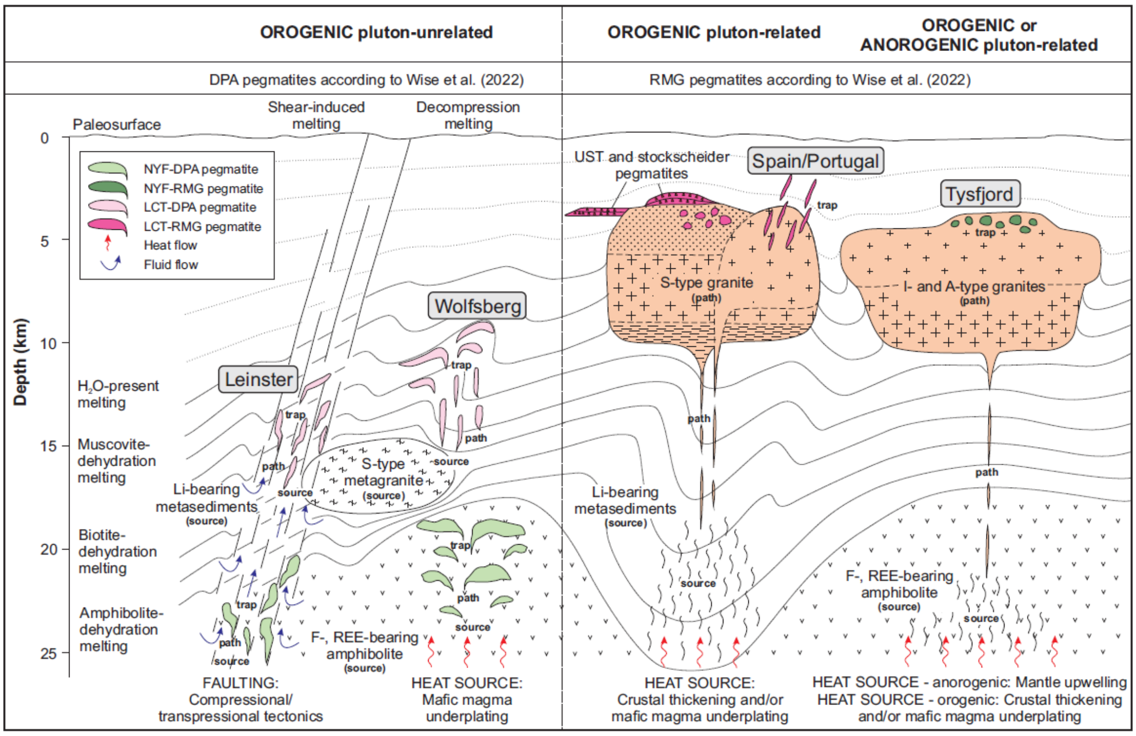

Fig. 3.1: Schematic crustal profile illustrating the contrasting controls on the formation of pegmatites in an RMG (pluton-related) compared with a DPA (pluton-unrelated) scenario. For DPA pegmatites, the source-rock composition, degree of partial melting, and subsequent fractionation processes control the formation of barren or mineralized pegmatites. The source LCT-DPA pegmatites can be Li-rich metasediments or S-type metagranites. Source: Modified from Müller et al. (2022) in Müller et al. (2025).

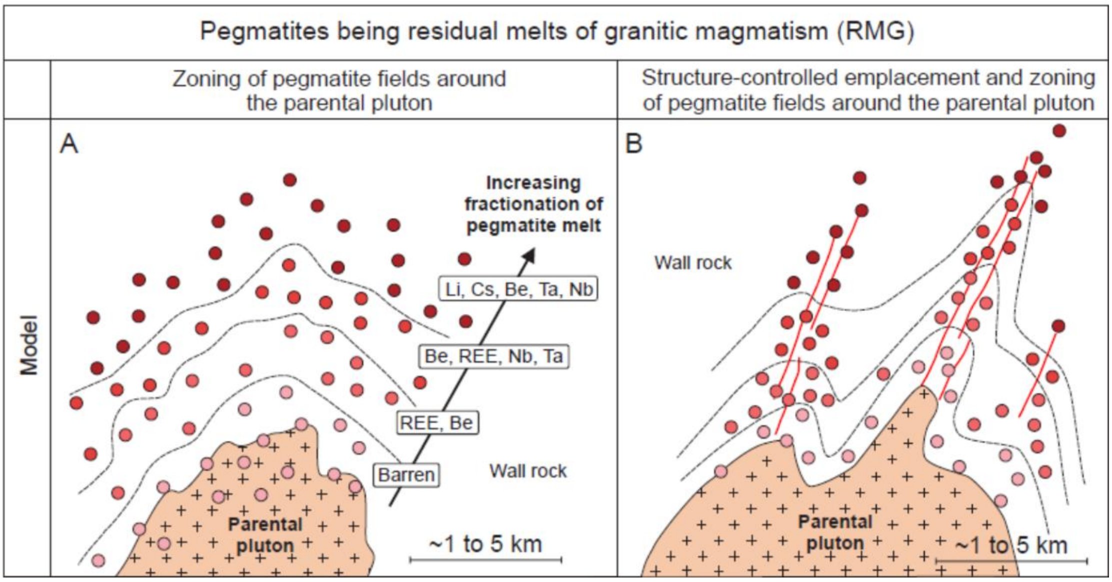

Fig. 3.2: District-scale chemical zoning of pluton-derived pegmatite fields (RMG). The colored dots represent pegmatite occurrences. **A)** Model of a concentric chemical zoning of a pegmatite field around the parental pluton. Modified from Černý (1991b). **B)** Model of a field where pegmatite emplacement is strongly controlled by tectonic structures and the melts increasingly modified owing to fractionation as they migrate along structures away from the parental granite. Source: Modified from Černý (1991b) in Müller et al. (2025).

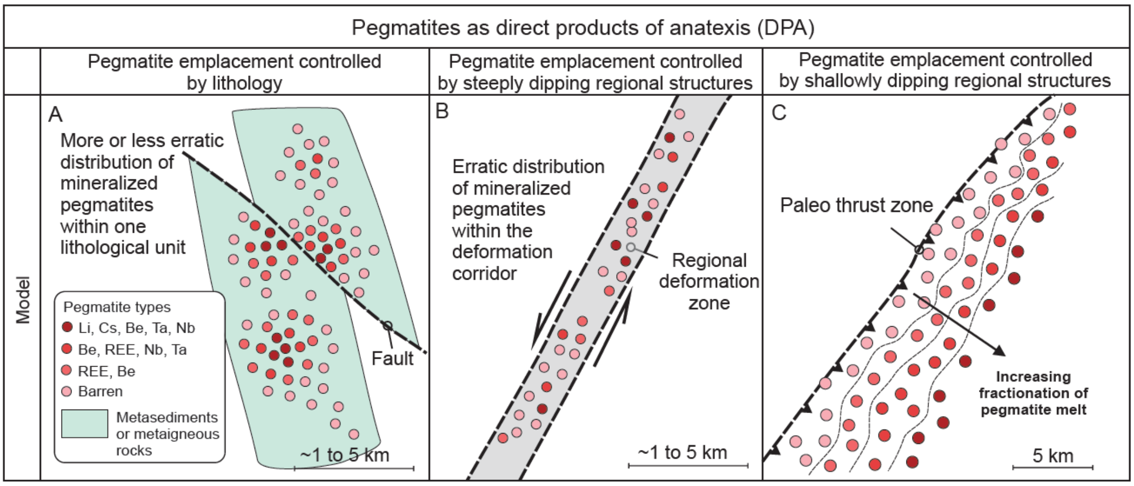

Fig. 3.3: District-scale chemical zoning of pegmatite fields formed by direct products of anatexis (DPA). The colored dots represent pegmatite occurrences**.** **A)** Model of a pegmatite field situated in one lithological unit (rock type). **B)** Model of a pegmatite field bound to major, steeply dipping tectonic structure. **C)** Model of a zoned pegmatite field above a shallowly dipping paleothrust zone. Source: Modified from Müller et al. (2015) in Müller et al. (2025).

3.4 Classification and Zoning

LCT pegmatites (Černý, 1991a) or Group 1 pegmatites (Wise et al., 2022) are rich in lithium (Li), cesium (Cs), and tantalum (Ta), hence the acronym LCT. These elements can reach concentrations high enough to be mined economically. Other valuable elements often found include tin (Sn), beryllium (Be), rubidium (Rb), and occasionally phosphorus (P). LCT pegmatites typically form from melts generated through partial melting of metasedimentary rocks, classifying them as S-type. They are commonly hosted in metamorphic rocks of greenschist to amphibolite facies, or in S-type granites.

NYF pegmatites (Černý, 1991a) or Group 2 pegmatites (Wise et al., 2022), named for their typical enrichment in niobium (Nb), yttrium (Y), and fluorine (F), can also contain rare earth elements (REEs), which behave chemically like yttrium, as well as thorium (Th), which may pose disposal challenges due to its radioactivity. These pegmatites originate from partial melting of igneous or metaigneous rocks, either in anorogenic (A-type, often alkaline) or I-type settings. They are commonly found in metamorphic rocks (greenschist to amphibolite facies) or in A- and I-type granite plutons.

Wise et al. (2022) also identify a less common group of I-type pegmatites, formed from metaigneous sources with enrichment in elements such as B, Be, REEs, Nb, Ti, Li, Ca (groups 1 and 2) or Al, Be, B (group 3). These typically occur in higher-grade metamorphic terrains (amphibolite to granulite facies) but are not discussed further here due to their rarity.

Another group, known as simple, barren, ceramic, or abyssal pegmatites, is also recognized. The term “barren” is relative, it may only refer to the absence of a specific target element. For instance, a pegmatite without lithium minerals like spodumene or petalite might be considered barren for lithium yet still be economically valuable for feldspar.

The previously discussed pegmatite classifications are summarized in Table 1 below.

Table 3.1: Chemical, Mineralogical, and Genetic Classification of Granitic Pegmatites. Classifications according to Wise et al. (2022) with reference to the NYF-LCT pegmatite family grouping by Černý (1991a); quartz and feldspars are not named because they occur in all granitic pegmatites. Source: in Müller et al. (2025).

	Granitic pegmatites as residual melts of granite magmatism (RMG)					
	Group 1—LCT (S-type granite melt-derived)		Group 2—NYF (A-type granite melt-derived)		Groups 1 and 2—LCT and NYF (I-type granite melt-derived)	
Rock-forming	Biotite Almandine Muscovite	Fe, Mg Al	Biotite Fayalite Arfvedsonite/ riebeckite Magnetite Spessartine Muscovite	Fe, (±Mg) Mn Al	Biotite Almandine Muscovite	Fe, Mg Al
Rare element	Schorl Beryl Columbite-group Tapiolite-(Fe) Wodginite Cassiterite Graftonite group Amblygonite-montebrasite Triphylite-lithiophilite Elbaite Lepidolite Spodumene Pollucite	B Be Nb, Ta, Sn P P, Li, F P, Li Li, B Li, F Li Cs	Allanite Gadolinite Fergusonite Samarskite Euxenite Columbite-group Monazite Xenotime Beryl Phenakite Zinnwaldite Topaz Fluorite Cryolite	REE, Y, Be, Nb Ta, P Be Li, Fe F	Schorl Beryl Columbite-group Allanite Monazite/xenotime Topaz Fluorite Elbaite Liddicoalite Lepidolite Danburite Hambergite Epidote Stilbite/laumontite	B Be Nb, Ta REE, Y, Nb, Ta P F Li, B, Ca Be, B Ca
Additional accessories	Apatite Cleavelandite Zircon		Aegirine Amazonite Amethyst Ilmenite Helvine group	Hyalite opal Molybdenite Schorl Triplite Zircon	Amazonite Amethyst Anatase Apatite Axinite Cleavelandite Ilmenite Kunzite	Petalite Pollucite Pyrochlore group Rhodizite Stilbiotantalite Titanite Zinnwaldite Zircon
	Granitic pegmatites as direct products of anatexis (DPA)					
	Group 1—LCT (anatectic)		Group 2—NYF (anatectic)		Group 3 (anatectic)	
Rock-forming	Biotite Almandine Muscovite	Fe (±Mg) Al	Biotite Magnetite Hornblende Almandine Muscovite	Fe, (±Mg) Al	Cordierite Kyanite Andalusite Sillimanite Muscovite	Mg Al
Rare element	Schorl Beryl Amblygonite-montebrasite Lepidolite Spodumene Elbaite Pollucite	B Be P, Li, F Li, F Cs	Uraninite Allanite Monazite/xenotime Titanite Beryl Columbite-group	U REE, Nb P Ti Be Nb, Ta	Schorl Dumortierite Grandidierite Borasilite Chrysoberyl	B Be
Additional accessories	Apatite Cleavelandite Columbite-group Cassiterite Graftonite group Triphylite-lithiophilite	Petalite Zircon	Amazonite Epidote Fluorite Hematite Ilmenite	Molybdenite Schorl Topaz Zircon	Almandine Beryl Corundum Gahnite Ilmenite	Monazite Rutile Sapphirine Surinamite Zenotime Zircon

3.4.1 LCT Pegmatites (Group 1)

Many LCT pegmatites exhibit internal mineral and textural zoning, with crystal size typically increasing toward the core (Jahns, 1955 in Müller et al., 2025). Common zones include a medium-grained border, granophyric wall, blocky intermediate zone, quartz core, and late-stage replacement zones (Fig. 3.5A). However, economically significant albite-spodumene pegmatites in some areas are often poorly zoned or unzoned, for reasons not yet fully understood (Fig. 3.5B). Layered structures observed in some Iberian pegmatites are attributed to rapid disequilibrium crystallization due to injection into open fractures and strong melt undercooling (Garate-Olave *et al.,* 2017; Roda-Robles et al., 2023 in Müller et al., 2025). Shallowly emplaced pegmatites (<2.5 kbar) may develop miarolitic cavities with gem-quality spodumene, tourmaline, beryl, and topaz.

Inward crystallization typically leads to (semi-)perpendicular crystal alignment relative to host rock walls (Černý and Ercit, 2005). Unzoned pegmatites often have randomly oriented crystals, possibly due to syntectonic intrusion or low undercooling conditions (Keyser et al., 2023a).

Many spodumene pegmatites exhibit a bimodal crystal size distribution. Coarse-grained primary spodumene, quartz, feldspars, and muscovite can be altered into finer-grained quartz–muscovite and albite assemblages. Cleavelandite (platy albite) may also crystallize directly from melt (Kaeter et al., 2018). Spodumene breakdown reduces the lithium potential, but albitization may enhance Sn and Ta potential, as secondary albitite may host cassiterite and tantalite-columbite minerals. Tantalite-columbite in albitized zones tends to be more Ta-rich than those in the primary assemblage (Kaeter et al., 2018, 2021).

Geochemical halos commonly form due to fluid expulsion during intrusion and/or crystallization. They show enrichment in B, Li, Rb, Cs, Be, Sn, Ta, and Nb (Barros et al., 2022; Errandonea-Martin et al., 2022), with variations in spatial extent from centimeters (Geiger et al., 2024) to tens of meters. These halos may be visible within ~10 cm of contacts or detected in drill core. Minerals hosting the halo signature include micas, tourmaline, amphiboles, and Nb-Ta–rich oxides. Halo development is influenced by host-rock properties, melt chemistry, fluid content, depth of emplacement, and rock rheology (Barros et al., 2022; Errandonea-Martin et al., 2022).

3.4.2 NYF Pegmatites (Group 2)

Enrichment in Nb, Y, and F results in crystallization of characteristic accessory minerals including allanite, gadolinite, fluorite, topaz, aeschynite, euxenite, fergusonite, and samarskite. Amazonite (green microcline) is a typical indicator (Martin et al., 2008). Higher Fe contents than LCT pegmatites lead to biotite, magnetite, and hornblende crystallization. These pegmatites may also be enriched in REEs, Be, U, and Th, sometimes referred to as REE pegmatites. High U, Th, and K levels can result in elevated gamma radiation.

The zoning is generally less pronounced than in LCT types. Some patterns include increasing crystal size inward and progressive enrichment in Li, Rb, Ta, and Cs in micas (Rosing-Schow et al., 2018 in Müller et al., 2025), and Rb in feldspar (Müller et al., 2008). Chemically evolved NYF pegmatites can display complex zoning, including granitic-textured borders, graphic quartz-feldspar intergrowths, megacrystic intermediate zones (rich in microcline), and massive quartz cores (>100,000 m³). Miarolitic cavities with gem-quality minerals can occur in shallow intrusions (<2.5 kbar).

Some evolved NYF pegmatites develop fine-grained albite (cleavelandite) replacement zones that overprint earlier textures and may be enriched in Li, Rb, Cs, Ta, and Sn-leading to misinterpretation as mixed NYF-LCT pegmatites (Müller et al., 2018).

Like LCT types, NYF pegmatites also produce halos during emplacement or crystallization. These halos are enriched in Rb, Tl, Li, Cs, Ta, F, Sn, Nb, U, and Th, extending meters from the pegmatite body.

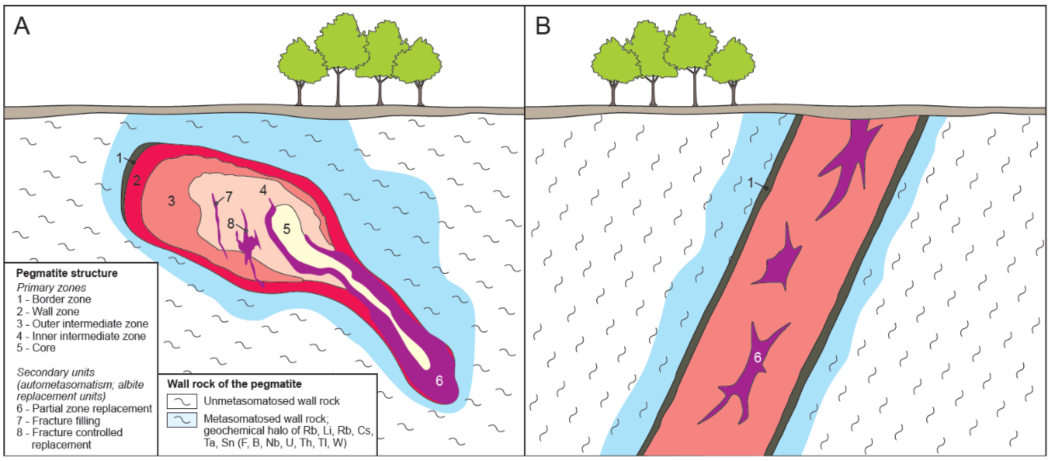

Fig. 3.4: Schematic diagrams of internal zoning and surrounding lithogeochemical halo in two contrasting styles of pegmatite body. **A)** Complexly zoned, stock-like pegmatite. From Jahns (1955), modified by Wise et al. (2022). **B)** Unzoned, dyke-like pegmatite with thin aplitic/granitic border zones. Source: Müller et al. (2025).

3.5 Spatial Organization of Pegmatites in the European Context

Pegmatites represent the smallest geological and mapping unit within pegmatite systems. However, when they occur in greater numbers or cover broader areas, they can be grouped hierarchically into fields, belts, or pegmatite provinces, based on shared structural, geochemical, and petrogenetic features (Černý, 1991b).

Pegmatite fields are localized areas typically less than 10 km², composed of multiple pegmatite dykes that are structurally and geologically interconnected; pegmatite belts consist of multiple fields aligned along major structural lineaments or shear zones; and pegmatite provinces encompass several belts and fields, generally located within the same metallogenic province. These provinces may contain pegmatites of different types, formed during various stages of crustal evolution, reflecting the tectono-magmatic complexity of the region (Černý, 1991b; Wise et al., 2022).

The map prepared by in Müller et al. (2025) for the GREENPEG project (Fig. 3.6) shows the main pegmatite provinces in Europe, classified according to the dominant pegmatite types, based on melt-generation mechanisms and geochemical enrichment styles (DPA-LCT, RMG-LCT, DPA-NYF, RMG-NYF). Notable observations include that the Variscan province, covering parts of the Iberian Peninsula, France, and Germany (regions 14 to 17), hosts mostly RMG-LCT and DPA-LCT pegmatites, linked to the partial melting of metasedimentary or granitic sources. In Scandinavia, provinces such as Tysfjord (nº 9) and Kola-Karelia (nº 1) are dominated by NYF-type pegmatites, both DPA and RMG, associated with metaigneous sources and A-type granites. The Alpine domain (region 19) features a variety of pegmatite types, mirroring the region's complex geotectonic and crustal evolution.

This hierarchical organization of pegmatite bodies is essential in mineral exploration, as it helps predict the pegmatite type and, consequently, the economically valuable elements present, such as Li, Ta, Nb, REEs, or Be.

The study area of the present work is located within the RMG-LCT pegmatite province (nº 16).

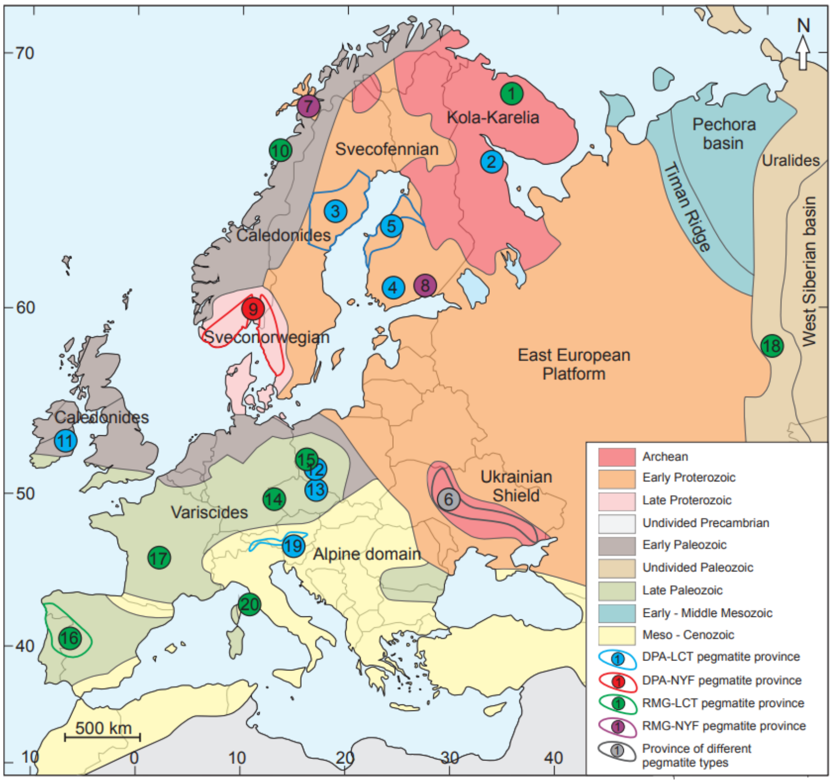

Fig. 3.5: Simplified geologic map of Europe with locations of major pegmatite provinces and fields. Pegmatite provinces (see also Table 6): 1 = Kolmozero-Voronja, Kola, 2 = Northern Karelia, 3 = Bothnian Basin, 4 = Somero-Tammela, 5 = Kaustinen, 6 = Ukrainian Shield, 7 = Tysfjord, 8 = Wiborg-rapakivi granite-related pegmatites, 9 = South Scandinavian, 10 = Meloy- Glomfjord, 11 = Leinster, 12 = Góry Sowie, 13 = Dolní Bory-Hate, 14 = Hagendorf-Pleystein, 15 = Strzegom, 16 = Central Iberian zone and Galicia-Trás-Os-Montes zone, 17 = Massif Central, 18 = Alabashka, Central Urals, 19 = Austroalpine unit, 20 = Elba. Source: Müller et al. (2025).

Chapter IV

Geological Setting

4.1 Introduction

The geological framework of the Iberian Peninsula can be categorized into four major groups, based on their age and tectonic history: (1) Precambrian terrains affected by pre-Palaeozoic deformation; (2) Palaeozoic terrains intensely deformed during the Variscan orogeny; (3) Mesozoic and Tertiary terrains that experienced deformation related to the Alpine orogeny; and (4) Mesozoic and Tertiary terrains that remained unaffected by Alpine tectonics (Julivert et al., 1974). Structurally, the Iberian Peninsula is composed of two principal domains: one representing the continuation of the European Variscan Cordillera, and another forming part of the Alpine orogenic front.

The Iberian Massif, which represents the westernmost fragment of the European Variscan Belt, can be subdivided into the following zones of contrasting lithologically, structural and/or metamorphic characteristics: Cantabrian Zone (CZ), West-Asturian-Leonese Zone (WALZ), Galicia-Trás-os-Montes Zone (GTMZ), Central Iberian Zone (CIZ), Ossa-Morena Zone (OMZ) and South Portuguese Zone (SPZ) (Julivert et al., 1974; Ribeiro et al., 1979; Farias, 1987), represented in the figure 4.1.

The study area belongs to the Barroso-Alvão Aplite-Pegmatite Field, situated in the Trás-os-Montes region, in northern Portugal. Geotectonically, it is positioned in the northwestern portion of the Iberian Massif, within the parautochthonous metasedimentary units of the GTMZ, specifically to the west of the Régua-Verín Fault.

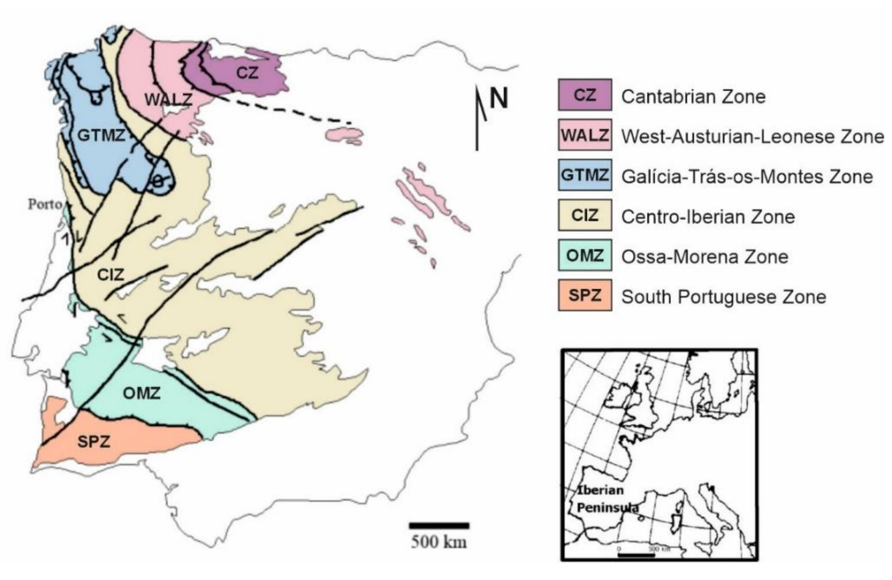

Fig. 4.1: Geotectonic zones that constitute the Iberian Massif as defined by Julivert et al. 1974, and Farias et al., 1987. Map on the right locates the Iberian Peninsula in Europe. Source: Modified from Quesada, 1991 in Correia, 2021.

4.2 Tectonism and Deformation

According to Dias & Ribeiro (1995), the Iberian Massif was affected by the Variscan orogeny, which began in the Devonian and extended into the Carboniferous. This tectonic event impacted different regions of the Iberian Peninsula in distinct ways. The main deformation phases and the orientation of structures vary between the Northern Sector, which includes the CZ, the WALZ, GTMZ, and the CIZ; and the Southern Sector, comprising the OMZ and the SPZ, represented in Fig. 4.2.

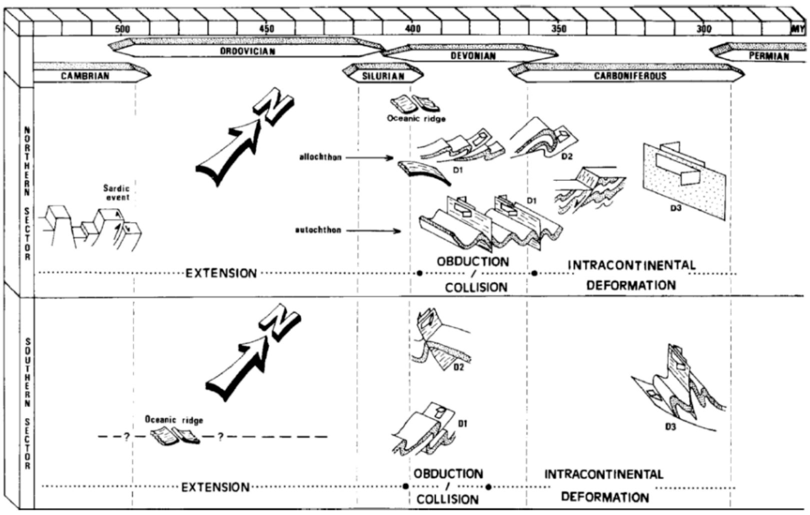

Fig. 4.2: Timing of the main deformation events in the Northern sector and the Southern sector of the Iberian Peninsula. After a period of extension there is an obduction/collision period commencing in the Devonian that corresponds to the Hercynian cycle, responsible for the major deformation observed in the field. Source: Dias & Ribeiro, 1995.

The GTMZ, where the study area is located, corresponds to a tectonometamorphic zone formed during the Variscan Orogeny. This orogenic event is characterized by a sequence of three major deformation phases (D_1, D_2, and D_3), which produced three generations of foliation in the host rocks of the aplite-pegmatite veins (Martins et al., 2006; Sant'Ovaia et al., 2011).

The Variscan Belt resulted from the continental collision between Laurasia and Gondwana, leading to the closure of the Rheic Ocean and the development of a complex nappe structure composed of multiple overthrusted crustal units. These nappes, separated by major thrust faults, constitute the architecture of the GTMZ.

The boundary of the GTMZ is defined by a major D_2 thrust fault, which emplaced both allochthonous and parautochthonous nappes over the autochthonous sequences of the Douro Inferior Domain, part of the CIZ (Noronha et al., 2006).

The D_1 phase produced folds with predominant NW-SE orientation, characterized by steep axial planes and an early planar fabric (S_1 foliation). In the parautochthonous units, these structures were later reworked by D_2 deformation (Ribeiro, 1998).

D_2 phase maintained a deformational style consistent with D_1, but imposed a southeastward vergence, forming tight, asymmetrical and overturned folds with a short limb. In the parautochthonous units, this phase led to the rotation and flattening of S_1, generating a crenulation cleavage (S_2) (Ribeiro, 1998).

The D_3 phase is associated with open folds of small amplitude, generally with vertical axial planes, and with the development of vertical ductile shear zones. At the regional scale, the parautochthonous domains exhibit D_3-related folding with subhorizontal hinges and subvertical axial planes trending between N100° and N120° (Ribeiro, 1998).

Following D_3, the region underwent a period of ductile–brittle to brittle deformation (late-D_3 to post-D_3), marked by the formation of conjugate fracture systems trending NNE-SSW and NNW-SSE, the former being more prominent. A key structure associated with this phase is the Régua-Verín Fault, initially formed during D_3 and later reactivated as a strike-slip fault. This fault juxtaposes two crustal levels: a deeper one to the west and a shallower one to the east (Noronha,1983; Ribeiro, 1998; Sant'Ovaia et al., 2011).

In addition to the host metasedimentary rocks, the Variscan deformation also affected some of the dykes themselves, folding them and indicating late-stage tectonic overprinting. It is also noteworthy that some dykes exhibit evidence of late-stage shearing, suggesting reactivation during post-emplacement deformation events.

In the Barroso-Alvão aplite-pegmatite field, several aplite-pegmatite dykes were emplaced along structural axes associated with the third deformation phase (D_3). The emplacement of these dykes is largely controlled by the dominant S_2 foliation, although in certain sectors they locally exploit S_3-related weakness zones, and in some cases, the dykes themselves are folded by D_3 structures (Lima, 2000).

4.3 Metamorphism

The Central Iberian Zone (CIZ) and the Galicia-Trás-os-Montes Zone (GTMZ) have undergone intense regional metamorphism and widespread granitic plutonism. According to Martínez et al. (1990), several metamorphic zones have been delineated for the Iberian Massif, marked by isograd boundaries that reflect a complex metamorphic evolution. These isograds often display crosscutting relationships, indicating the overprinting of multiple metamorphic events. The most recent of these events is attributed to the intrusion of two-mica S-type granites.

The Barroso-Alvão aplite-pegmatite field is located within a prograde metamorphic zone, characterized by low to medium pressure and high-temperature conditions, likely associated with the emplacement of syn-tectonic intrusion, the Cabeceiras de Basto granite, and late-tectonic granites. In this area, the metamorphic isograd runs parallel not only to the granite contact but also to the surrounding lithostratigraphic boundaries (Ribeiro et al., 2000).

Mineralogical assemblages observed in the field suggest that the study area lies within the andalusite metamorphic zone (Ribeiro et al., 2000), as evidenced by the presence of the following parageneses:

i) quartz + muscovite + biotite +/- andalusite +/- staurolite;

ii) quartz + muscovite + biotite +/- andalusite +/- staurolite +/- garnet +/- plagioclase.

In the work of Martins (2009), the author reports that the biotite isograd was also identified as being subparallel to the andalusite isograd, and is characterized by the following three mineral assemblages:

i) quartz + muscovite + biotite;

ii) quartz + muscovite + biotite + chlorite;

iii) quartz + muscovite + biotite + albite +/- chlorite +/- garnet.

According to Lima (2000), the presence of the biotite zone, controlled by a syn-F_3 syncline, on one hand, and the occurrence of andalusite crystals deformed by D_3 folds on the other, suggest that the metamorphic climax was reached prior to the final phase of Variscan deformation. Therefore, the regional metamorphism appears to decrease in intensity away from the Cabeceiras de Basto granitoid massif, following a trend that transitions from the andalusite zone into the biotite zone, and then returns again to the andalusite zone.

4.4 Metasediments

The metasedimentary rocks in study area were examined in detail by Ribeiro et al. (2000), who subdivided the sequence into three distinct formations: unit S^a, unit S^b, and unit S^c, based on metamorphic conditions and lithological associations. Later, Ribeiro et al. (2007) compared units S^a, S^b, and S^c to the sequences located east of the Vila Real

Fault, which had been previously characterized by Ribeiro (1998). In the present study, the entire area of investigation is fully encompassed within unit S^b, indicating that the lithologies and metamorphic conditions observed are characteristic of this formation (Fig. 4.3).

From a lithostratigraphic, lithochemical, and structural perspective, the parautochthonous units of the GTMZ are characterized by metasedimentary and vulcano-sedimentary rocks from the Ordovician to the Devonian; and are subdivided into two distinct domains, separated by the Palheiros-Vila Flor thrust fault. These domains are referred to differently depending on the geological map sheet: in Sheet 6-C of the Geological Map of Portugal (scale 1:50000), they are labeled as Lower Parautochthonous and Upper Parautochthonous; in Sheet 6-D, the same units are designated as the Três Minas Structural Domain (TMSD) and the Carrazedo Structural Domain (CSD), respectively (Ribeiro et al., 2000; Sant'Ovaia et al., 2011).

The Três Minas Structural Domain (TMSD) corresponds to the lowermost tectonic nappe within the parautochthonous assemblage and is also referred to as the Lower Parautochthonous. Within this domain, two well-defined lithostratigraphic units can be distinguished, each exhibiting markedly different lithological characteristics: the Fragas Negras Unit (S_{FN}) and the Curros Unit (D_{CU}). However, within the Barroso-Alvão aplite-pegmatite field, located west of the Régua-Verín Fault, only the S_{FN} is clearly identified. This unit is correlative with the autochthonous units of the Marão region, such as the Campanhó Formation, and corresponds to the S^a unit on the 6-C geological map sheet.

The Fragas Negras Unit (S_{FN}) is composed predominantly of quartz-phyllites and gray to black phyllites, interlayered with lidytes, which may locally and laterally transition into gray quartzites. Additionally, it occasionally includes intercalations of calcsilicate rocks and black carbonates. This unit is particularly characterized by a high content of organic matter, especially within its more argillaceous, siliceous, and carbonate-rich layers.

Regarding the Carrazedo Structural Domain (CSD), also west of the Régua-Verín Fault, only the Rancho Sub-unit (S_{Ra}). and the Santa Maria de Emeres Unit are distinguishable. These correspond, respectively, to units S^b and S^c on the 6-C sheet.

The Rancho Sub-unit (S_{Ra}) is distinguished by the predominance of dark-colored lithologies, mainly black schists, occasional lydite, and grey phyllites. As in the Fragas Negras Unit (S_{FN}), lateral transitions into grey quartzites are observed. This sub-unit also comprises intercalated calcsilicate horizons, banded quartz-feldspathic rocks, and occurrences of acid metavolcanic rocks.

The Santa Maria de Emeres Unit comprises a mixture of feldspathic bands, black schists, lidytes, phyllites, calcsilicate rocks, quartzites, and acid metavolcanic rocks (Noronha et al., 2006; Sant'Ovaia et al., 2011).

4.5 Granitic Rocks

The area encompassing the Barroso-Alvão pegmatite field hosts a diverse range of granitic rocks, including post-tectonic biotite granitoids with calcic plagioclase (e.g., Vila Pouca de Aguiar and Gerês), syntectonic two-mica granites (e.g., Cabeceiras de Basto complex, Serra do Barroso, and Chaves), and syntectonic two-mica granitoids with dominant biotite (e.g., Vila Pouca de Aguiar and the Barroso-Alvão Dome) (Lima & Noronha, 2006).

The continental collision during the D_1 and D_2 phases led to crustal thickening, enhanced by the overthrusting of crustal nappes. This tectonic regime facilitated the formation of syn-D_3 syntectonic granites through crustal anatexis, which intruded the cores of D_3 antiforms. These granites are typically two-mica leucogranites, muscovite-dominated, formed at mesocrustal levels from wet, peraluminous magmas, and are closely linked to regional metamorphic processes. Their internal fabric is commonly marked by a S_3 foliation trending NW-SE.

The association between metamorphism and syntectonic/tardi-tectonic granites in the study area is particularly evident. These granites generally exhibit elongated NW-SE shapes, parallel to the regional structural trend. Along the Cabeceiras de Basto granite and south of the Fragas Negras Unit, regional metamorphic isograds are observable, aligned both with igneous contacts and lithostratigraphic boundaries, reflecting the thermal peak related to late-D_3 to syn-D_3 deformation within a prograde dynamo-thermal evolution. This metamorphic evolution is marked by the early formation of staurolite relative to andalusite, and by the presence of andalusite and cordierite poikilitic textures formed during late- to post-tectonic stages.

The post-tectonic biotite granitoids with calcic plagioclase typically form elongated massifs that exploit deep fractures generated at the end of D_3 to intrude. These granites are thought to have originated at deep crustal levels, are subalkaline, and generally intrude the upper crust, as their dry magma composition allows longer transport distances. An example of this granite type is the Vila Pouca de Aguiar granite (Noronha et al., 2006; Sant'Ovaia et al., 2011).

The Barroso-Alvão aplite-pegmatite field fits within this tectono-magmatic framework, displaying a spatial association between granites, migmatites, shear zones, and aplite-pegmatite veins. These veins are classified according to Cerný and Ercit (2005) as rare-element pegmatites of the LCT family (Li, Cs, Ta), with complex structures and the petalite and spodumene subtypes.

In the study area, numerous aplite-pegmatite veins appear to be structurally controlled by pre-existing foliations and D_3-related planes, striking between N-S to N40º and N150º. These features suggest that the opening of space for the emplacement of the pegmatitic magmas was associated with the third Hercynian deformation phase (D_3) within the metasedimentary host rocks, characterized by a sub-horizontal S_2 schistosity (Lima, 2000).

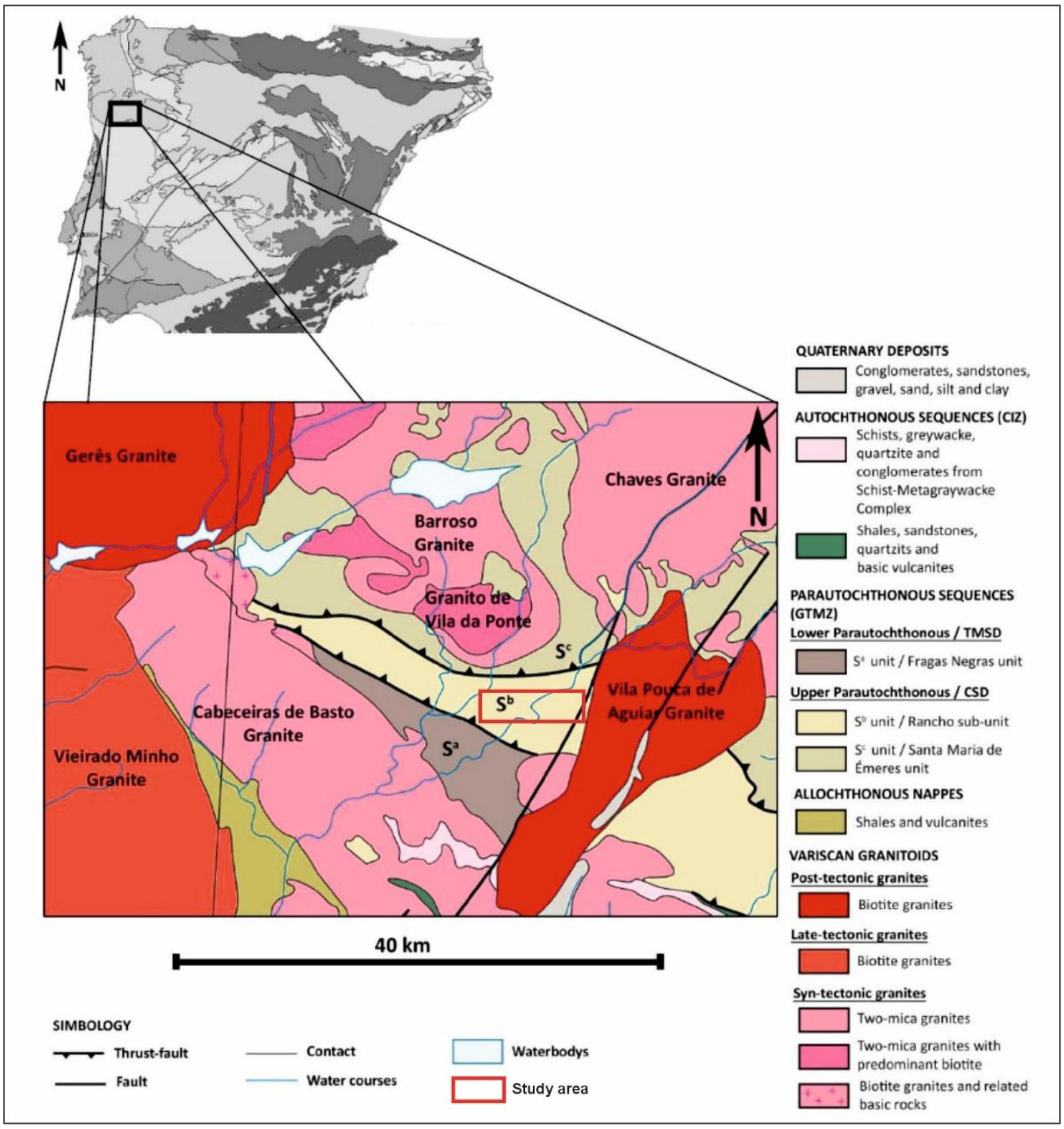

Fig. 4.3: Geologic map of the study area located in Barroso-Alvão aplite-pegmatite field. The study area of this work marked in red is fully inserted in the unit S^b. Source: Adapted from Dias (2011).

Chapter V

Field work and Validation

5.1 Introduction

In general, pegmatites tend to exhibit low thorium (Th) concentrations, a characteristic that can be attributed to their highly evolved magmatic nature and specific mineralogical composition. During the fractional crystallization of granitic magmas, Th, although an incompatible element, tends to be incorporated early into accessory phases such as monazite, allanite, or zircon, which typically crystallize before the late stage pegmatitic fluids. As a result, these fluids, which give rise to pegmatites, are often depleted in Th (cf. Černý, 1991; Simmons & Webber, 2008). Furthermore, pegmatites commonly lack thorium-bearing minerals in significant amounts, particularly in the case of LCT pegmatites, where the geochemical enrichment is largely focused on elements such as Li, Cs, Nb, and Ta (Černý, 1991a). This compositional signature makes pegmatites easily distinguishable from the surrounding host rocks in airborne radiometric surveys, as they frequently correspond to negative anomalies in thorium concentration maps.

Based on the aerial radiometry data provided by the GREENPEG project and considering that the main objective of this study was to carry out field verification to validate the application of the radiometric geophysical method in the identification of pegmatite bodies, zones of negative anomalies in the thorium (Th) concentration map were investigated. Negative anomalies were defined using a reference threshold of Th concentrations less than or equal to 14.3 ppm. From these anomalies, ten research targets were delineated, within which 121 outcrop points were recorded and described, distributed across the areas identified as priorities for investigation, as shown in the map in Figure 5.1. Additionally, six supplementary outcrop points were mapped outside the main targets, serving as control locations to support geological correlation and to validate the broader applicability of the geophysical interpretation.

In addition, two radiometric profiles were carried out in two distinct research targets, aiming to complement the geophysical interpretation with in-situ ground gamma-ray data. The instrument used for radiometric surveying is called a gamma-ray spectrometric. The one used in this study is the GR-320 Exploranium model, which is a portable spectrometer. For the ground radiometric data, negative anomalies were defined as thorium (Th) concentrations less than or equal to 10 ppm.

Outcrop Location Map

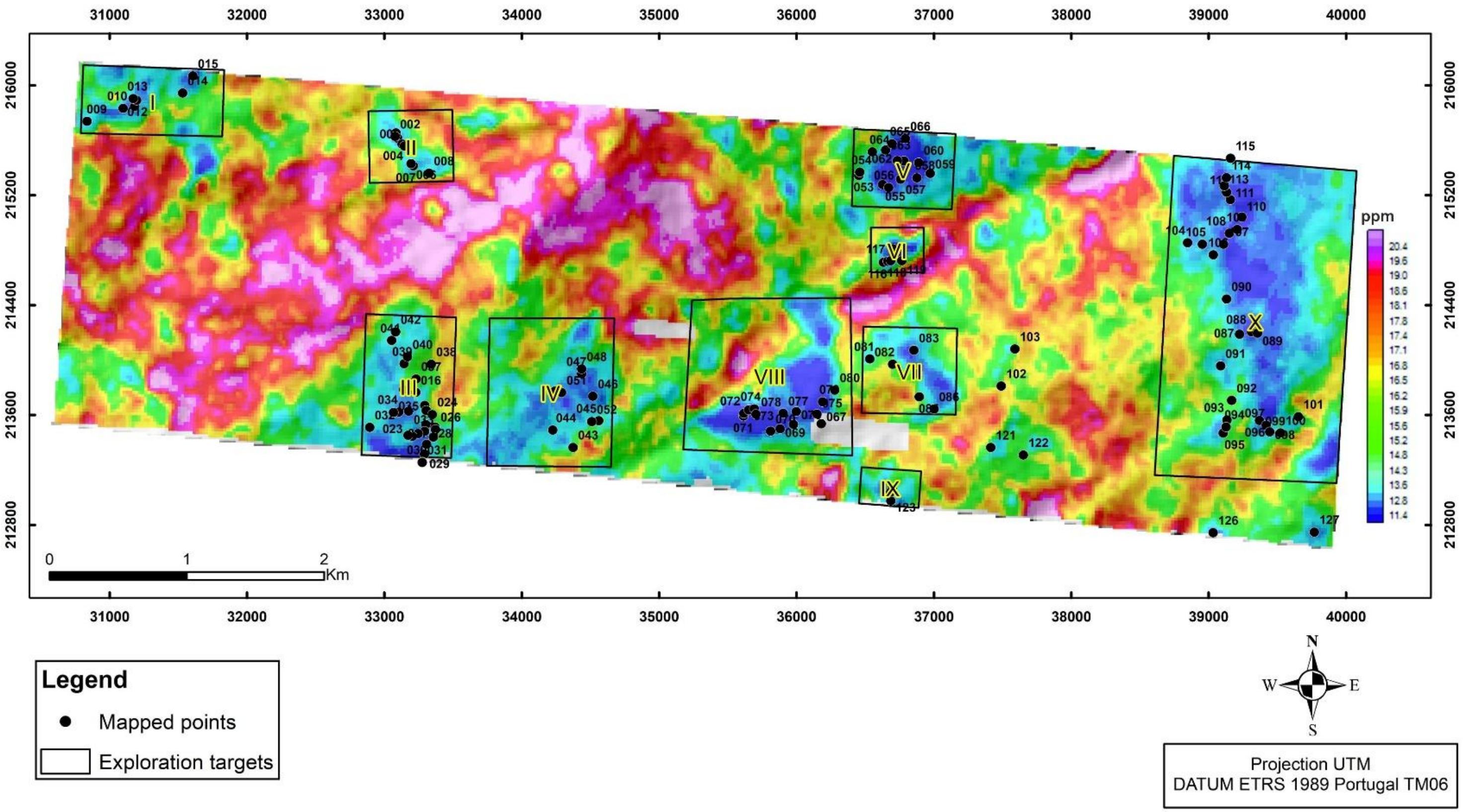

Fig 5.1: Map showing the distribution of mapped outcrop points and the delineation of research targets.

5.2 Results and discussions

5.2.1 Target I

At the first verification target, seven points were mapped (Fig. 5.2), six of which correspond to outcrops of metasedimentary rocks present in the area, and one to a pegmatite outcrop.

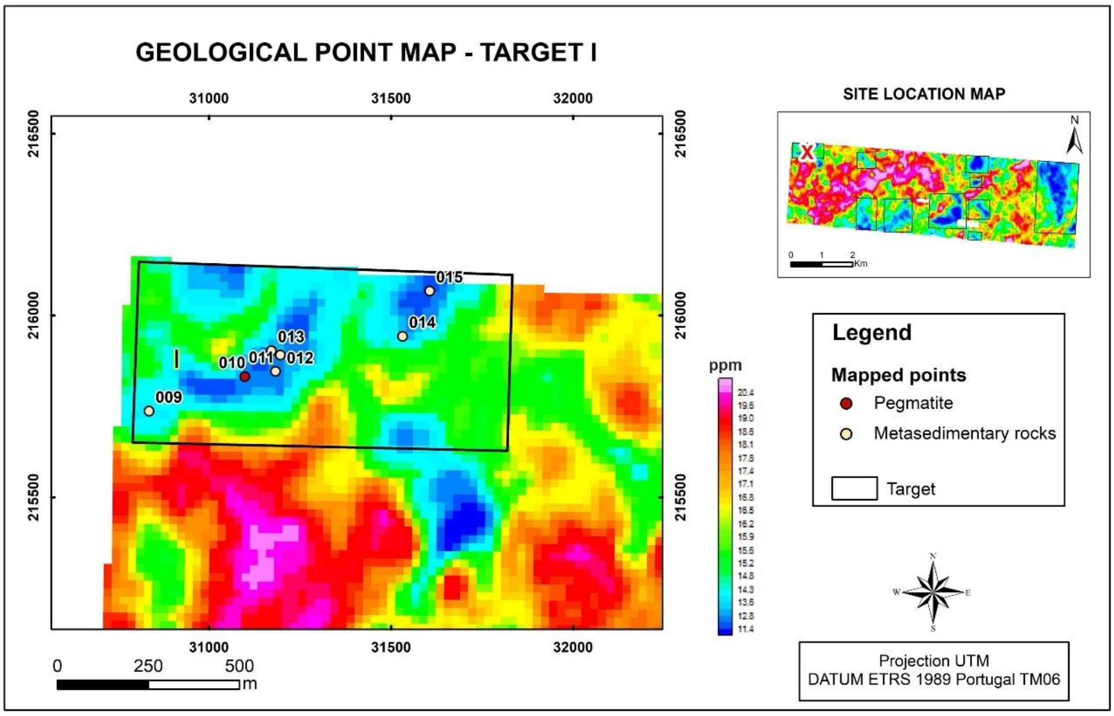

Fig 5.2: Geological point map focused on Research Target I. Thorium (Th) concentration map provided by the GREENPEG project.

A contact zone between the pegmatite and the metasediments was observed, with a direction following the foliation of the host rock, oriented at N120º (Fig. 5.3). The pegmatite appears to have been emplaced along a weakness zone generated during the D_3 deformational phase, exhibiting a sharp and subconcordant contact with the host rock.

At this target, the metasedimentary rocks are strongly deformed, with orientations ranging from N115° to N160°, indicating the presence of a shear zone associated with D_3. These data corroborate the observations by Lima (2000), who identified the metasedimentary rocks as being strongly affected by the D_3 phase, with preferential directions between N120° and N140°.

The mapped metasedimentary outcrops display numerous quartz veins, with thicknesses varying from millimetric to centimetric scale, and often intensely fractured.

Some of these veins were emplaced syn-D_3 and are therefore concordant with the S_2 foliation; others are folded and boudinaged, suggesting emplacement prior to the D_3 phase (Ribeiro, 1998).

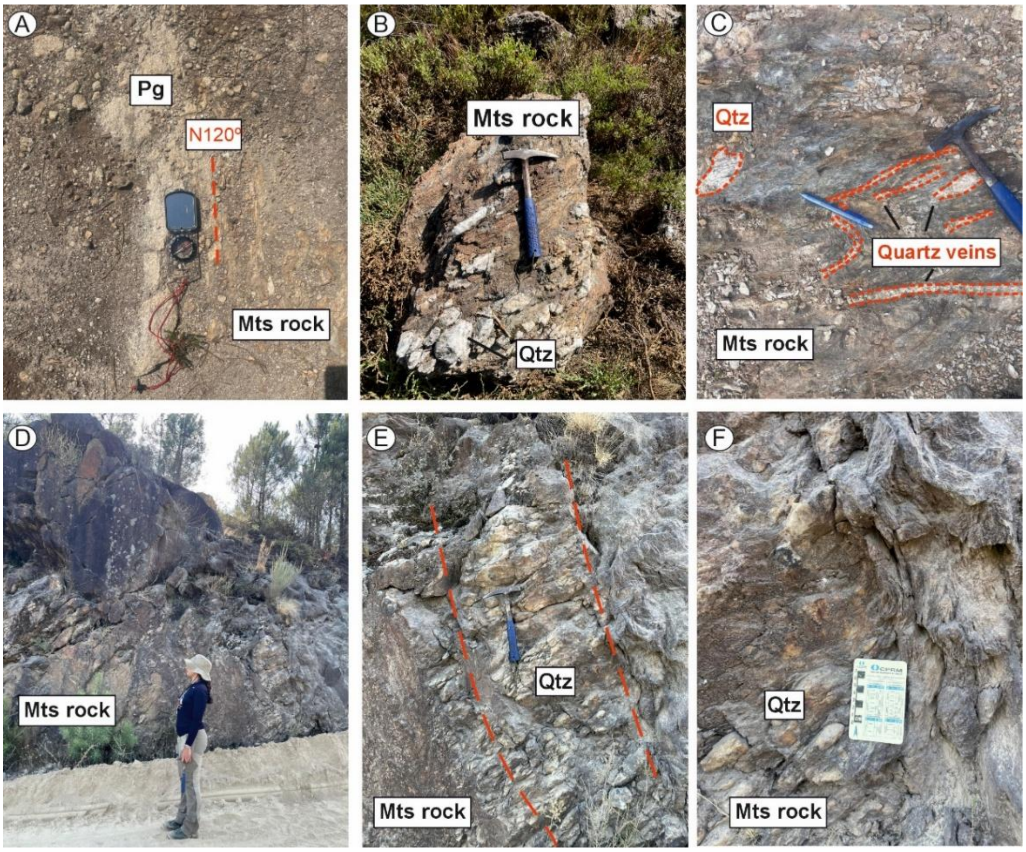

Fig 5.3: **A)** Contact between the pegmatite and the host metasediments, with orientation of N120º (Point 10). **B)** Metasedimentary rock block with centimetric quartz crystals. **C)** Metasedimentary rock crosscut by folded and boudinaged quartz veins. **D)** Metasedimentary rock outcrop at metric scale (Point 15). **E)** Intensely fractured quartz vein, approximately 1 m thick (Point 14), crosscutting the host rock. **F)** Quartz vein crosscutting the foliation of folded host metasedimentary rock (Point 14). Mts = Metasedimentary; Pg = Pegmatite; Qtz = Quartz.

As pegmatite outcrops in this target area are scarce, so ground geophysics was used as a complementary tool to assess the anomaly with greater precision. A radiometric profile of approximately 45 meters was carried out at Point 10, as shown in Fig. 5.4. The radiometric data indicated a negative anomaly for the element thorium (Th) in the points R2, R3, R5 and R6, suggesting the presence of a subsurface pegmatite body that is more extensive than what is exposed at the surface.

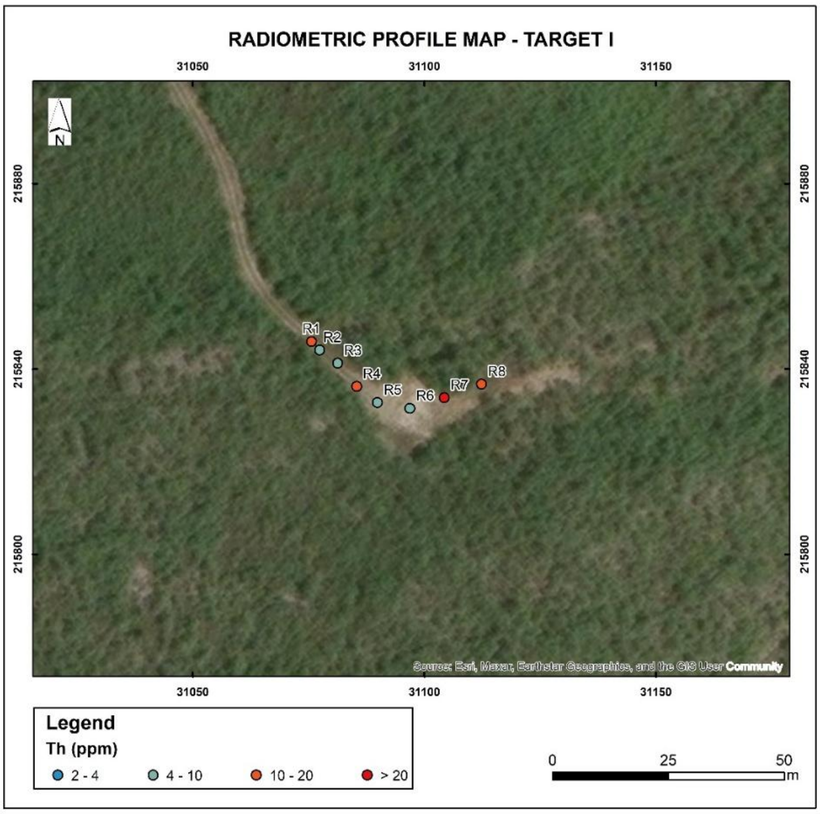

Fig 5.4: Radiometric profile map for target I.

Another factor that supports the reliability of the method is the observation, in the map shown in Fig. 5.1, of a strong negative anomaly located southeast of Target I. This anomaly corresponds to the Alijó aplite-pegmatite vein, which is extensively described in the literature (e.g., Noronha, 1987; Lima, 2000; Martins, 2009; Dias, 2016, among others). This pegmatitic body is known to be lithium-mineralised in the form of spodumene and is frequently referred to as the “spodumene pegmatites (type 4)” by Martins (2009) and as the “spodumene-bearing aplite-pegmatite dyke” by Dias (2016) (see Fig. 5.5).

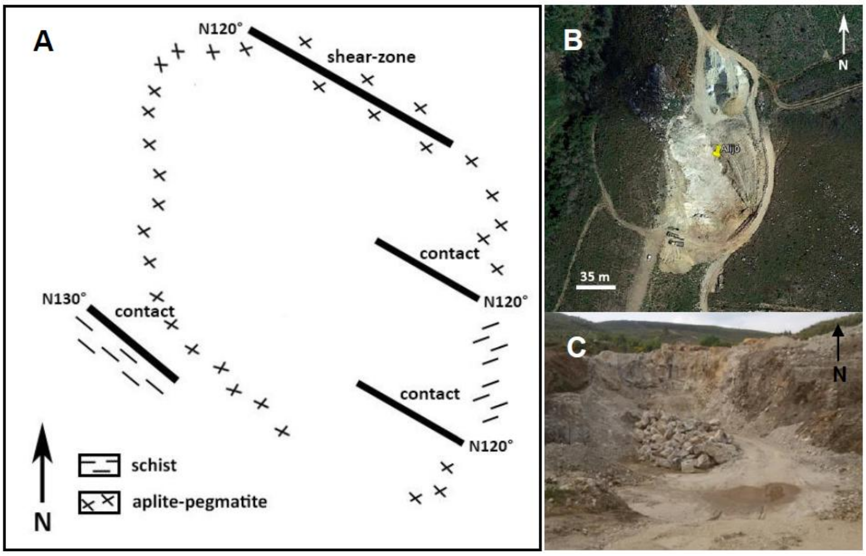

Fig 5.5 : Alijó aplite-pegmatite vein exploration site. **A)** Schematic figure representative of the contacts directions observed in the exploration site of the aplite-pegmatite vein and of a shear plane located north of the exploration. **B)** Satellite image of the exploration site. Google Earth adapted image. **C)** Exploration site photo. Source: Dias, 2016.

5.2.2 Target II

Research Target II (Fig. 5.6) exhibits lithological and structural characteristics similar to those observed in Target I, particularly regarding the host rocks and the orientation of their contacts with the pegmatites. However, a greater number of pegmatite outcrops were identified in this target, some of which display an aplitic texture, a common feature throughout the study area (Fig. 5.7).

In this target there are also pegmatitic bodies previously mapped on the Geological Portuguese map (sheet 6D, scale 1:50.000) and subsequently studied by Martins (2009), as well as occurrences of petalite mineralization.

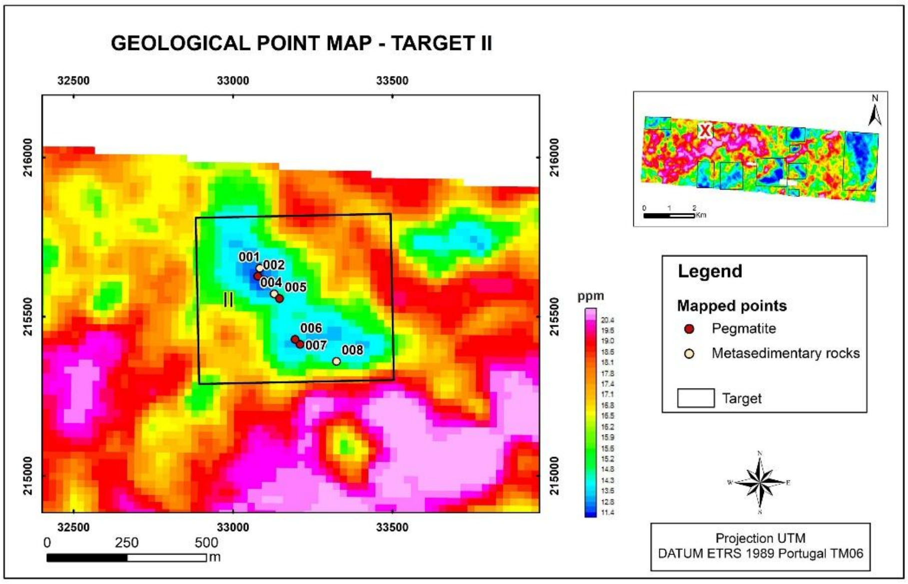

Fig 5.6*:* Geological point map focused on Research Target II. Thorium (Th) concentration map provided by the GREENPEG project.

Fig 5.7*:* **A)** Highly altered, poorly cohesive pegmatite exposed in a road cut. In the image, the soil color contrast highlights the boundary between the pegmatite body (white) and the host metasedimentary rocks (brown). (Point 6); **B)** Aplite-pegmatite outcrop (Point 5); **C)** Pegmatite sample displaying prominent K-feldspar crystals and manganese oxide. (Point 3); **D)** Meter-scale outcrop of metasedimentary rock similar to those observed at Target I. (Point 8); **E)** Contact between the pegmatite (Pg) and the host metasediments, with orientation of N115º (Point 7). Kfs = K-feldspar; Mn = Manganese oxide; Mts = Metasedimentary; Pg = Pegmatite; Qtz = Quartz.

5.2.3 Target III

At Target III (Fig. 5.8), a considerable number of pegmatites were also mapped (>10 bodies). These are concentrated both in the lower parts of the anomaly (blue zone) and in the higher portions (green zones; Points 37, 38 and 39), near the boundary considered for positive thorium anomalies. Macroscopically analysing their mineralogy, they are similar to those observed in the previous targets; however, from a structural perspective, many of these bodies exhibits strong presence of fractures (Fig. 5.9).

Furthermore, the N-S (N0°) contact orientation mapped at this target may correspond to a late-Variscan structural trend, that according to Lima (2000), these fractures generated during different stages of the Variscan orogeny could have acted as pathways that facilitated the emplacement of pegmatite bodies.

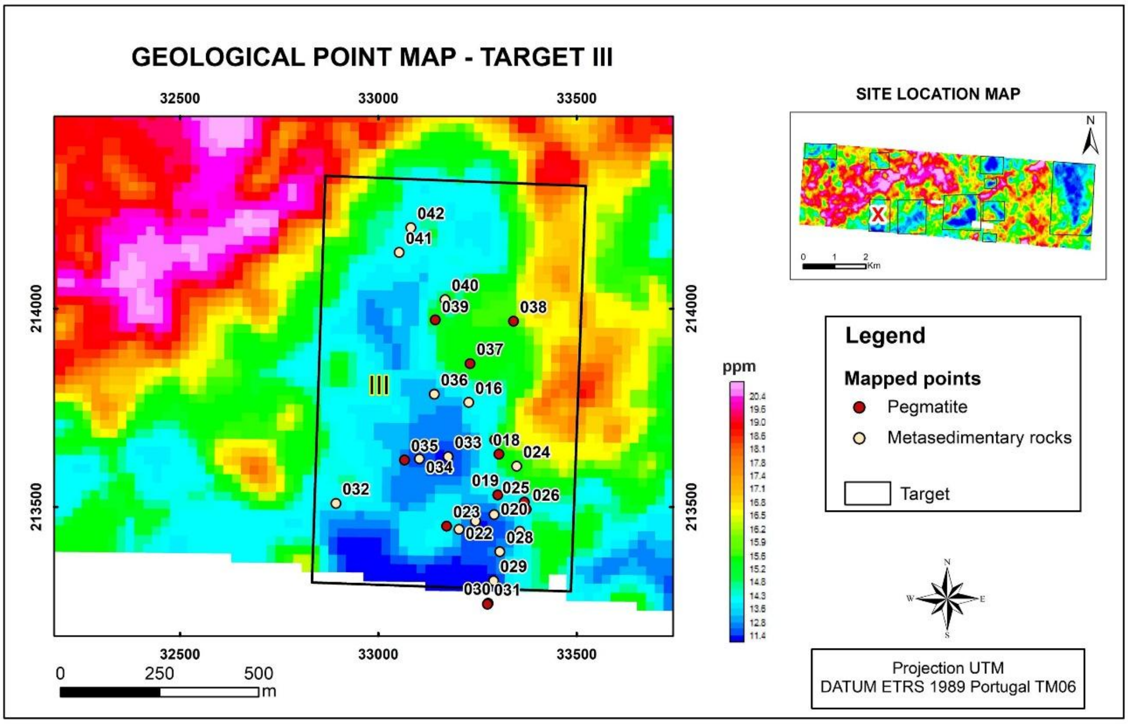

Fig 5.8: Geological point map focused on Research Target III. Thorium (Th) concentration map provided by the GREENPEG project.

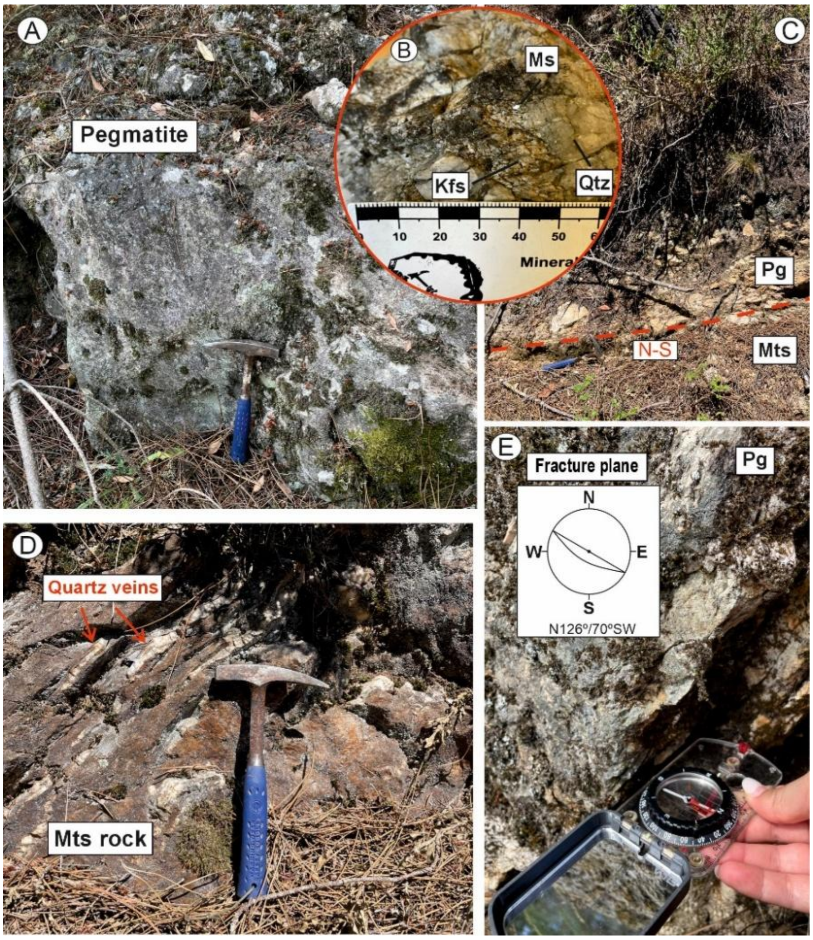

Fig 5.9: **A)** Meter-scale outcrop of pegmatite (Point 30); **B)** Pegmatite sample mineralogically composed by K-feldspar, muscovite and quartz (Point 31); **C)** Contact between the pegmatite and the host metasediments, with N-S orientation (Point 39); **D)** Metasedimentary rock with quartz veins (Point 40); **E)** Fracture-controlled pegmatite, with the main fracture orientation measuring N126°/70° SW (Point 26). Kfs = K-feldspar; Ms = Muscovite; Mts = Metasedimentary; Pg = Pegmatite; Qtz = Quartz.

5.2.4 Target IV

The pegmatites mapped at this target (Fig. 5.10) exhibit a more distinctly pegmatitic texture, characterized by visible centimetre-scale crystals of K-feldspar and quartz. A preferential alignment of crystals is also observed, suggesting a certain degree of structural organization within the body. This aligns with the explanation by London (1992), who states that as a hydrous silicate melt undergoes increasing liquidus undercooling, crystal growth evolves from a random orientation to a more organized pattern, frequently resulting in comb-like textures.

Regarding the host rocks, they also correspond to metasedimentary units, as observed in the previous targets. Although no quartz veins were identified at a visible scale, pegmatite veins were observed crosscutting these rocks (Fig. 5.11).

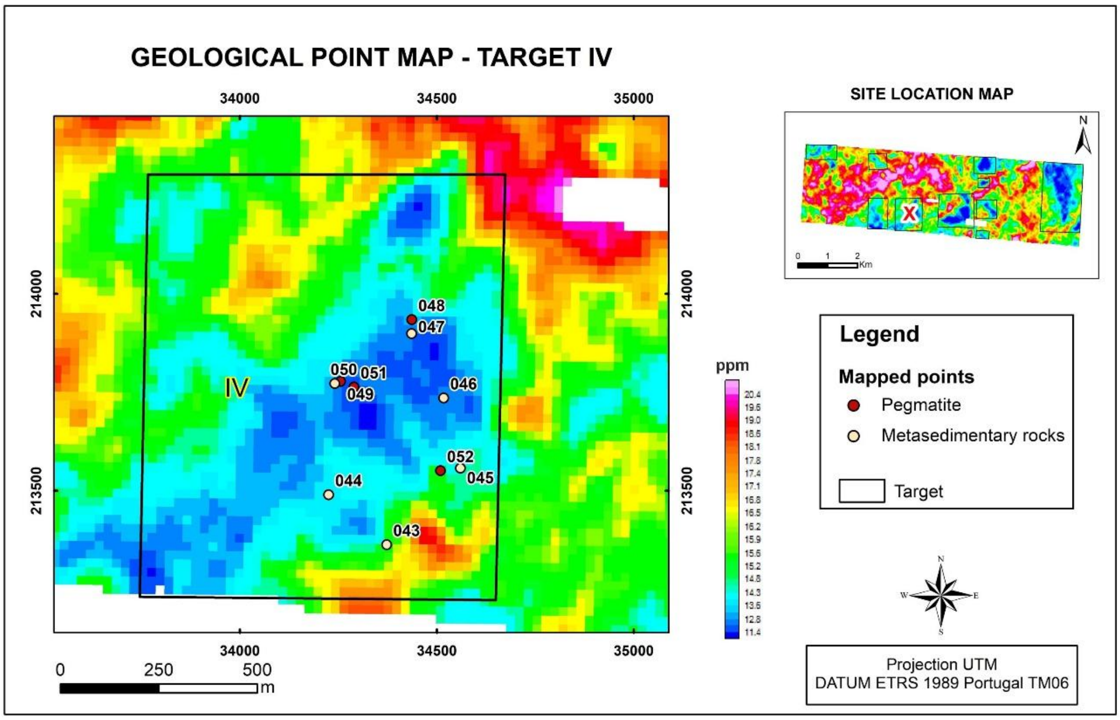

Fig 5.10: Geological point map focused on Research Target IV. Thorium (Th) concentration map provided by the GREENPEG project.

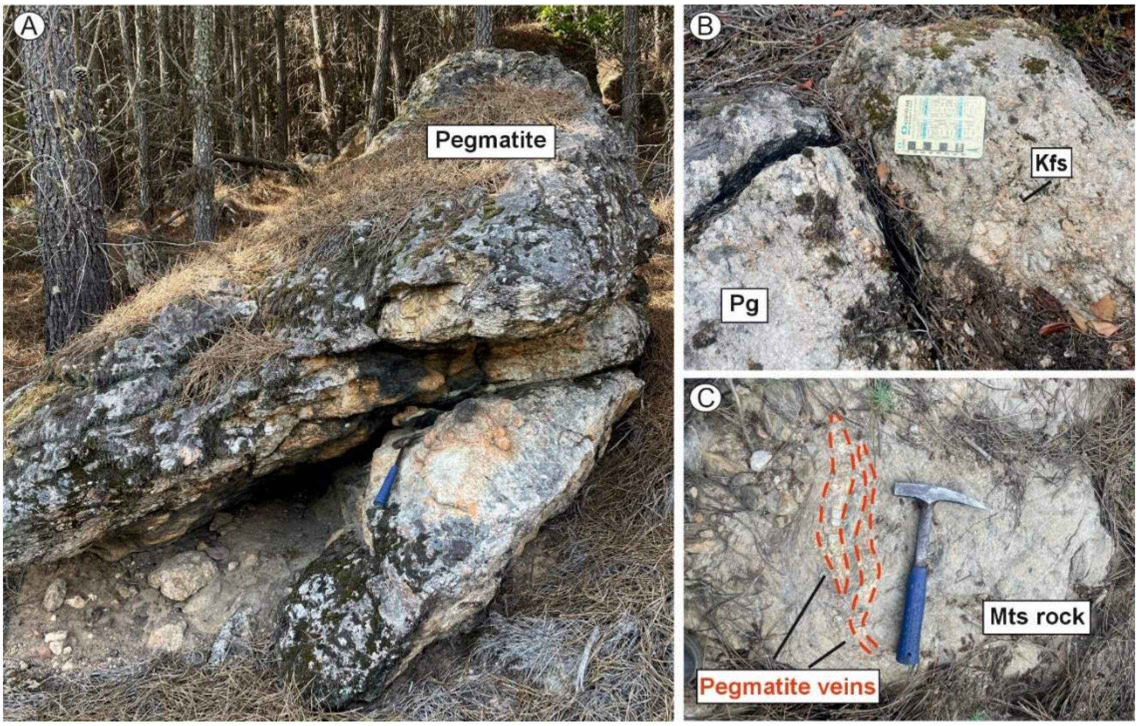

Fig 5.11: **A)** Metric-scale pegmatite blocks (Point 52); **B)** Pegmatite displaying centimetre-scale K-feldspar and quartz crystals with a preferential orientation (Point 48); **C)** Metasedimentary rock crosscut by pegmatite veins (Point 47). Kfs = K-feldspar; Mts = Metasedimentary; Pg = Pegmatite.

5.2.5 Target V

At Research Target V (Fig. 5.12), numerous pegmatite outcrops were mapped, both in the central portion of the anomaly and along its margins, as well as outcrops of the surrounding metasedimentary host rocks.

The pegmatites at this target predominantly occur as discrete blocks; however, in several instances, they were found in a highly weathered and poorly cohesive state, particularly at their contact with the also intensely weathered host rocks.

In the more preserved blocks, the pegmatites exhibit a well-developed pegmatitic texture, marked by centimetre-scale crystals of quartz and K-feldspar. Despite the advanced alteration observed in some exposures, K-feldspar crystals are still present near the contact zones with the surrounding metasedimentary rocks (Fig. 5.13).

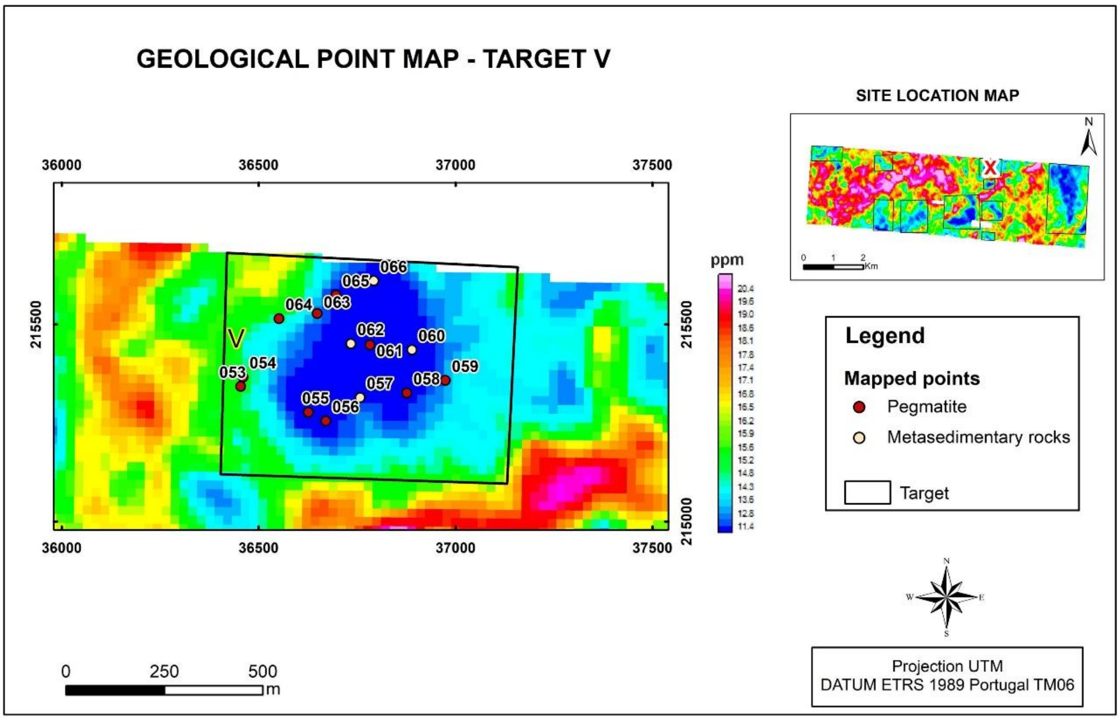

Fig 5.12: Geological point map focused on Research Target V. Thorium (Th) concentration map provided by the GREENPEG project.

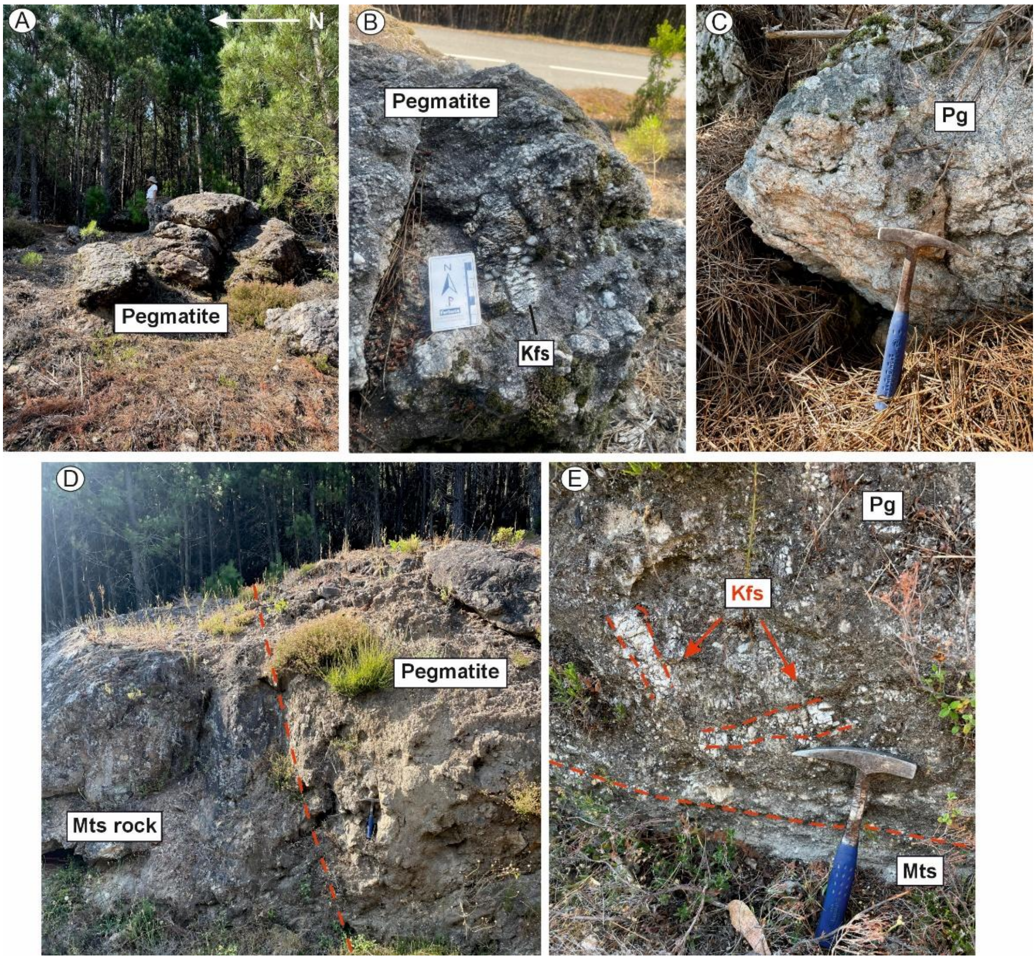

Fig 5.13: **A)** Overview of pegmatite blocks (Point 53); **B)** Detail of a pegmatite block showing centimetre-scale K-feldspar crystals; **C)** Pegmatitic texture within the pegmatite body (Point 63); **D)** Contact between the pegmatite and the metasedimentary host rock, both highly weathered (Point 56); **E)** Detail of K-feldspar veins near the contact zone between the pegmatite and the metasedimentary host rock (Point 56). Kfs = K-feldspar; Mts = Metasedimentary; Pg = Pegmatite.

At this target, a large pegmatite block in contact with metasedimentary rock was also mapped at Point 59 (Fig. 5.14). The orientation of the contact plane was measured at N150°/40°NE, appearing perpendicular to the foliation of the host rock. In this outcrop, it was also possible to observe the alternating occurrence of aplitic and pegmatitic textures, a distinctive feature of the Barroso-Alvão aplite-pegmatite field (Lima, 2000; Martins, 2009).

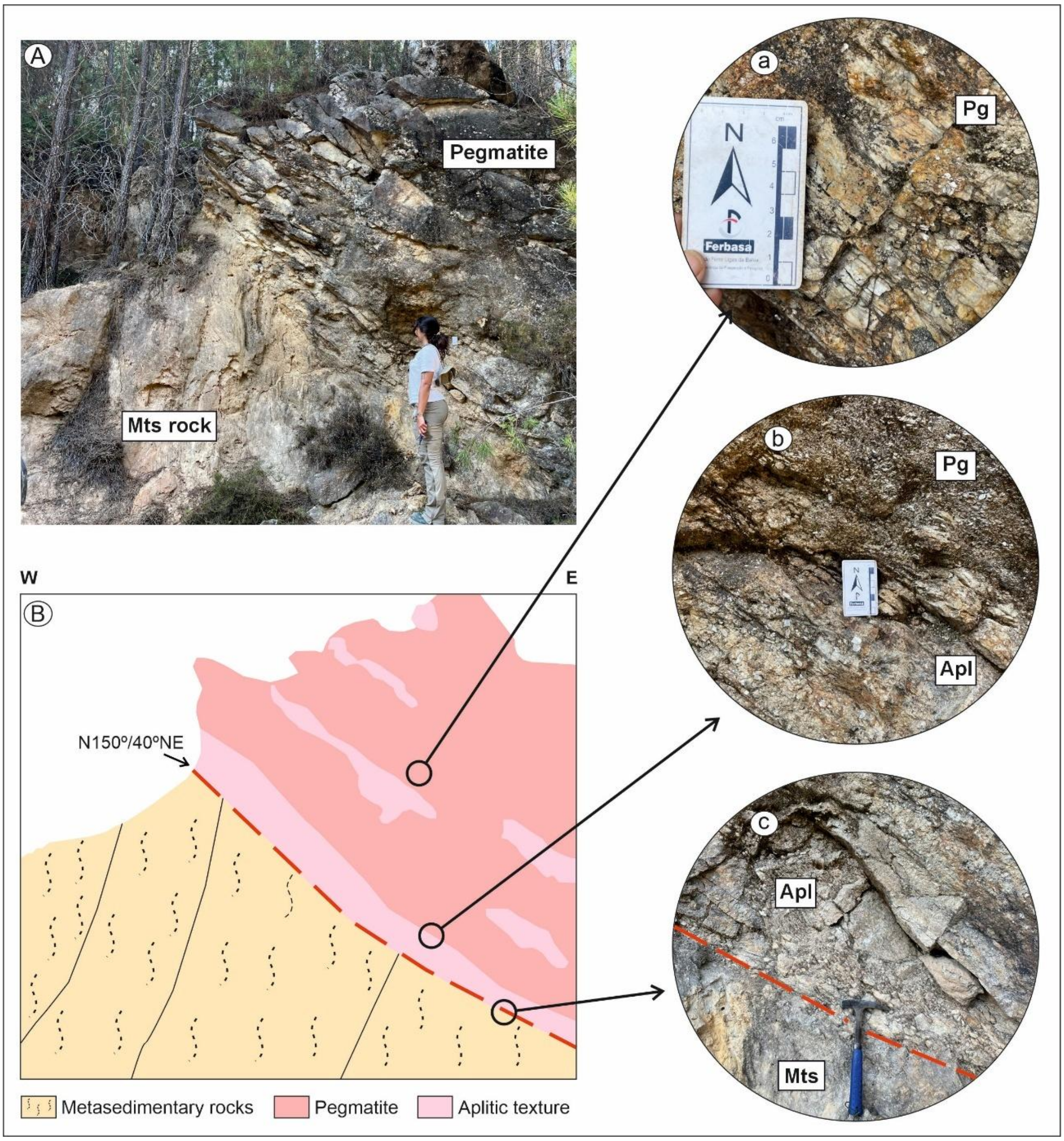

Fig 5.14: **A)** Metric-scale pegmatite block in contact with metasedimentary host rock, with the contact plane oriented N150°/40°N. **B)** Schematic representation of the outcrop; **a)** Detail of the pegmatitic texture; **b)** Detail showing the intersection between pegmatitic and aplitic textures; **c)** Contact zone between the metasedimentary host rock and the aplitic textures. (Point 59). Apl= Aplitic; Mts = Metasedimentary; Pg = Pegmatite.

5.2.6 Target VI

In this target area, three pegmatite outcrops were mapped (Fig. 5.15). These exposures reveal blocks containing K-feldspar crystals, as well as a strongly altered pegmatite outcrop in contact with similarly altered metasedimentary host rocks (Fig. 15.6). Additionally, Target VI includes an outcrop previously recorded on sheet 6D at a 1:50000 scale.

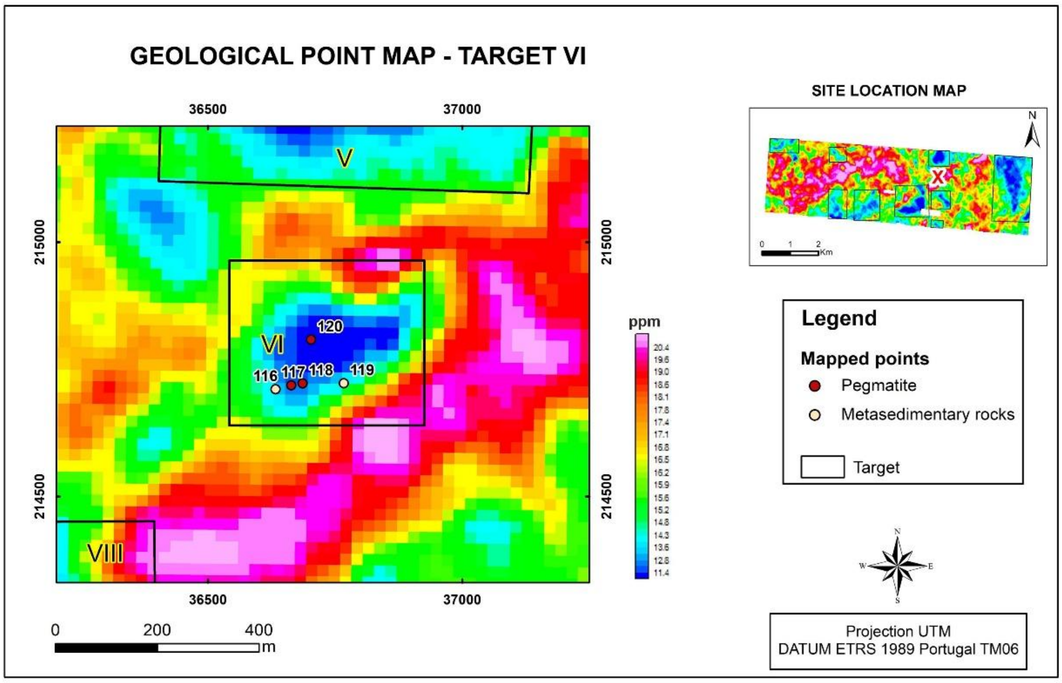

Fig 5.15: Geological point map focused on Research Target VI. Thorium (Th) concentration map provided by the GREENPEG project.

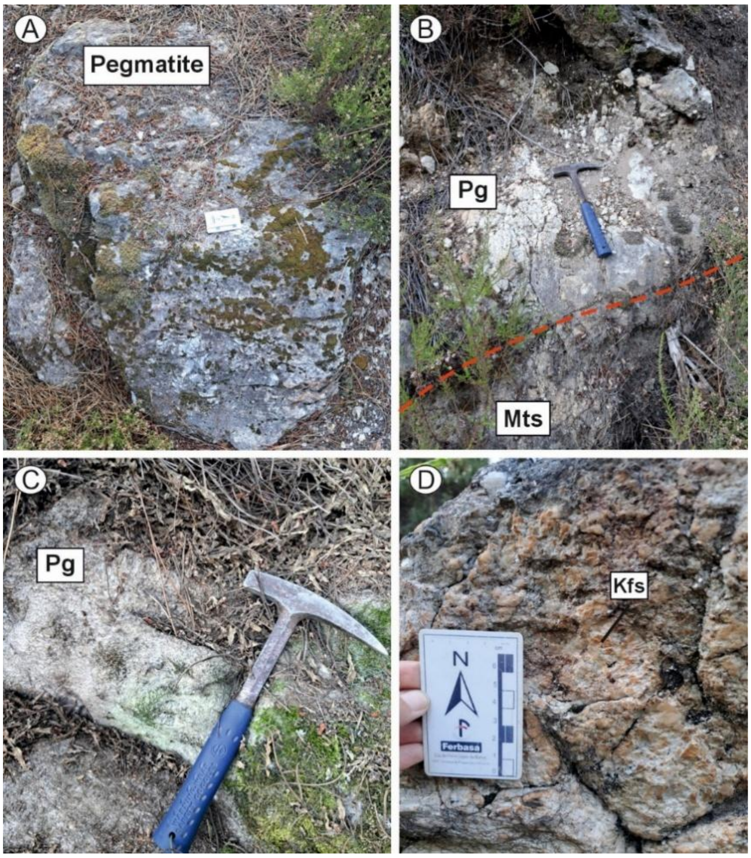

Fig 5.16: **A)** Pegmatite block (Point 120); **B)** Contact between pegmatite and the metasedimentary host rock, both strongly altered (Point 117); **C)** Detail of the pegmatite block (Point 121); **D)** Close-up view of K-feldspar in the pegmatite matrix. (Point 121). Kfs = K-feldspar; Mts = Metasediment; Pg = Pegmatite.

5.2.7 Target VII

At Target VII (Fig. 5.17), only a single pegmatite outcrop was mapped at the surface. The surrounding lithology is composed predominantly of metasedimentary rocks, which locally exhibit quartz veins ranging from millimetre to centimetre scale (Fig. 5.18). Despite the limited number of exposures, a radiometric profile was conducted across the target area to assess potential subsurface continuity (Fig. 5.19).

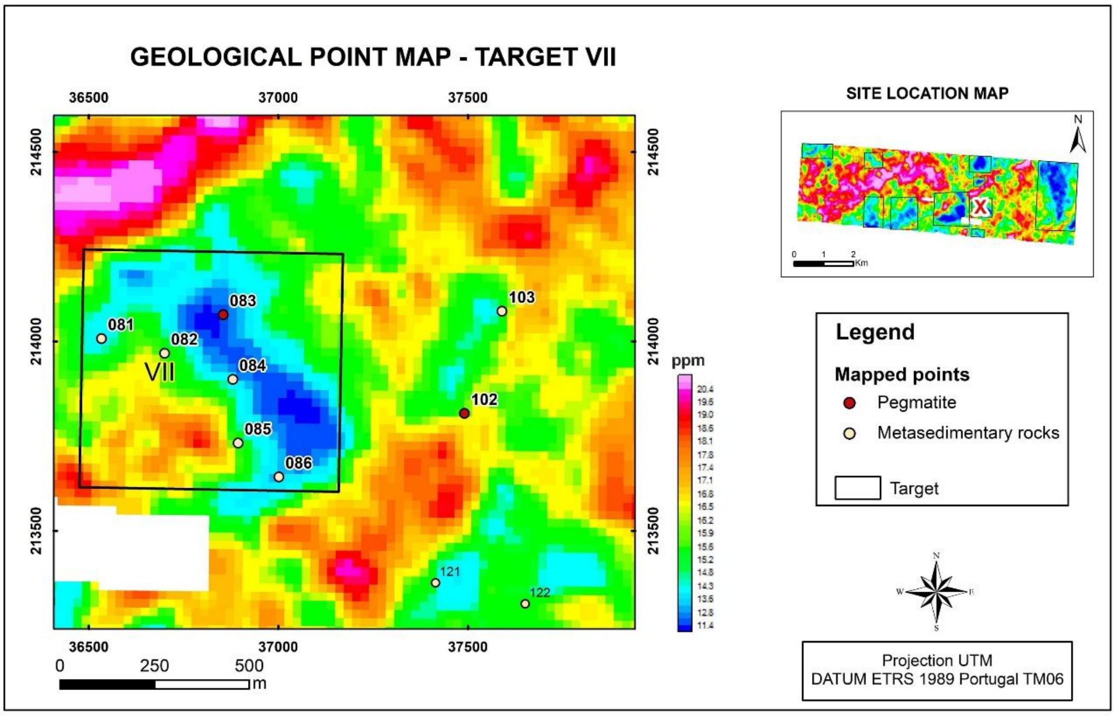

Fig 5.17: Geological point map focused on Research Target VII. Thorium (Th) concentration map provided by the GREENPEG project.

The radiometric data revealed Th values consistent with those typically associated with pegmatitic bodies in the study area (points R3-R8). This suggests the likely presence of additional pegmatite material at shallow depths, masked by weathering and limited surface exposure.

At Point 83, a direct contact between black schists and pegmatite was observed, further supporting the hypothesis of pegmatite intrusion into the local metasedimentary sequences. Moreover, this observation highlights a distinctive feature of the Rancho Sub-Unit (S_{Ra}), namely the presence of dark lithologies (Ribeiro, 1998; Sant'Ovaia et al., 2011). Although surface evidence is limited, the integration of radiometric data and field observations suggests a more extensive pegmatite presence in the subsurface at this target.

Another factor that may be contributing to the negative thorium (Th) anomaly observed in the radiometric data is the occurrence of black schists in the area. According to Schön (2015), black schists present an average Th concentration of 10.9 ppm, which is slightly lower than the values typically found in common schists (12 ppm). Although the difference is not particularly large, the predominance of black schists among the mapped lithologies may exert some influence on the radiometric response. This remains, however, a preliminary assumption, as no specific studies have been found to substantiate this interpretation in detail.

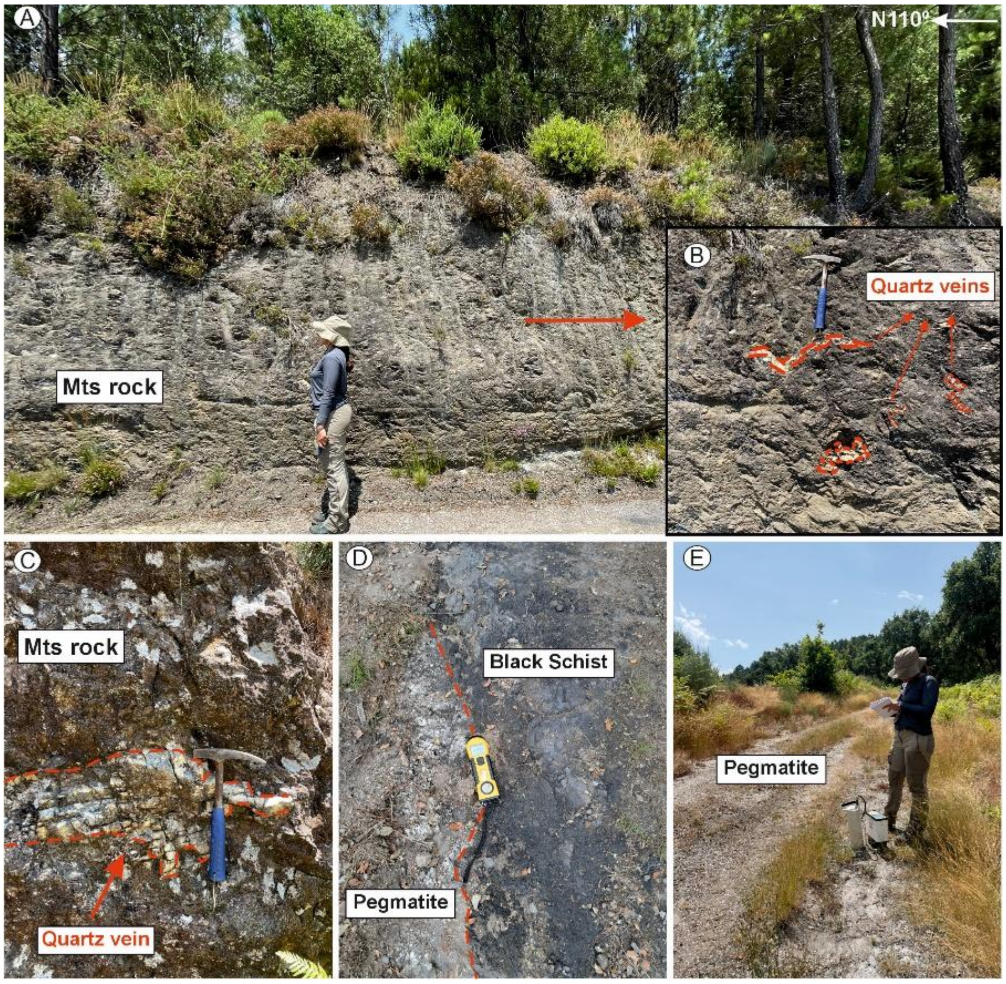

Fig 5.18: **A)** General view of the outcrop (Point 86); **B)** Detail of centimetre-scale quartz veins within the metasedimentary rock (Point 86); **C)** Detail of a quartz vein approximately 50 cm long crosscutting the metasedimentary rock perpendicular to its foliation (Point 85); **D)** Contact between pegmatite and black schist (Point 83); **E)** Radiometric data acquisition over the pegmatite body (Point 83). Mts = Metasedimentary.

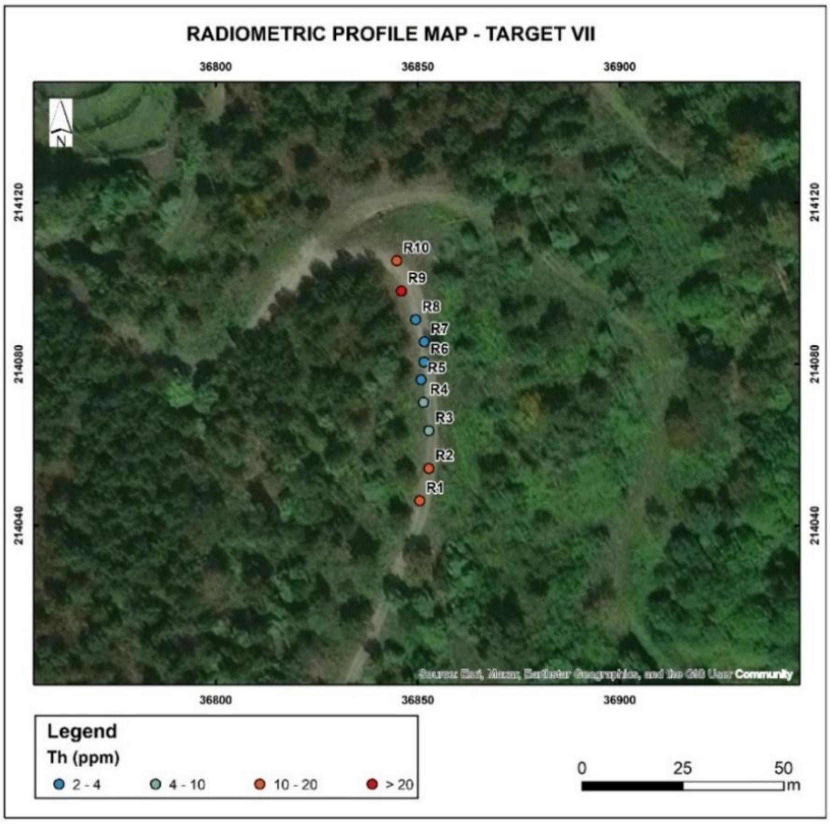

Fig 5.19: Radiometric profile map for target VII.

5.2.8 Target VIII

In Target VIII (Fig. 5.20), several pegmatite outcrops were identified, although most of the blocks observed were of relatively small size. These pegmatites display features consistent with those previously described in other target areas, including the presence of K-feldspar crystals, N-S oriented contacts, and subvertical dips toward the enclosing metasedimentary rocks (Fig. 5.21). According to Lima (2000), such geometries may be related to the F_3 dyke family and may reflect either the verticalization of the S_2 foliation during the D_3 deformation phase, or, more likely, the influence of late-stage shear zones.

The metasedimentary units also contain remnant K-feldspar crystals and quartz veins within their matrix. Furthermore, the presence of very dark metasediments was noted, potentially indicating the occurrence of black schist zones.

Target VIII is particularly noteworthy due to the presence of an extensive and intense radiometric anomaly. This observation is supported by the density of mapped pegmatite outcrops within the area. However, it is important to note that field observations revealed the presence of walls constructed with pegmatite blocks derived from human activity. This anthropogenic contribution may have influenced the anomaly, potentially accounting for its high intensity and spatial extent.

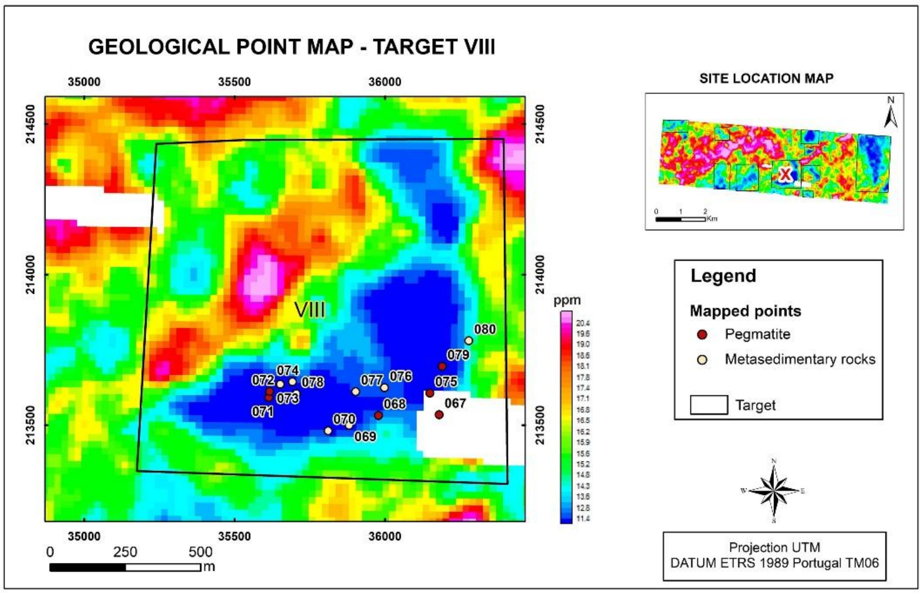

Fig 5.20: Geological point map focused on Research Target VIII. Thorium (Th) concentration map provided by the GREENPEG project.

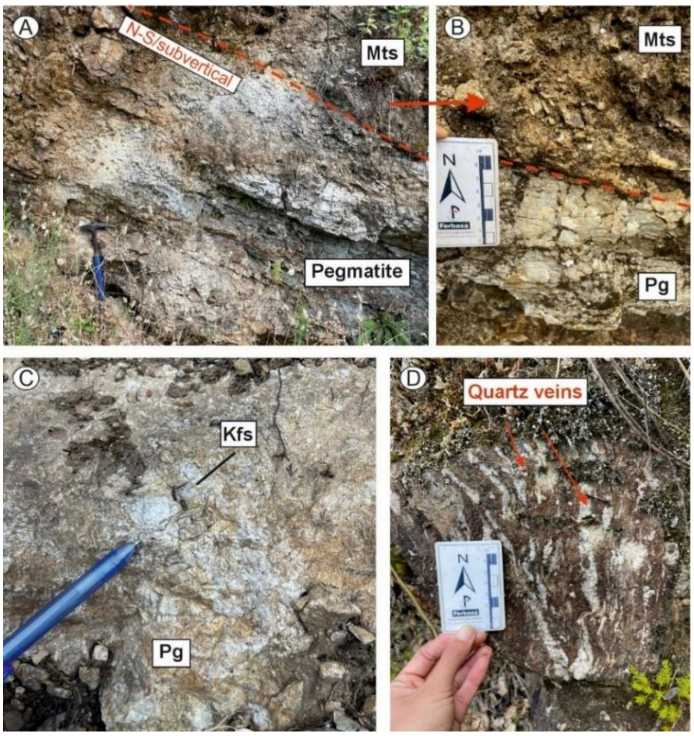

Fig 5.21: **A)** Contact between pegmatite and metasedimentary rock with N010º orientation and subvertical dip (Point 72); **B)** Detail of the contact, highlighting K-feldspar crystals within the metasediment (Point 72); **C)** K-feldspar crystals within the pegmatite (Point 68); **D)** Quartz veins hosted in the metasedimentary rock (Point 74). Kfs = K-feldspar; Mts = Metasedimentary; Pg = Pegmatite.

5.2.9 Target IX

At Target IX (Fig. 5.22), three outcrops were mapped, one of which reveals a well-defined contact between a pegmatite body and the surrounding metasedimentary rock. This contact displays a structural orientation of N40°W, indicating emplacement controlled by pre-existing anisotropies in the host rock, consistent with sub-horizontal D_2-related structures, which, according to Lima (2000), belong to the F_2 dyke family (Fig. 5.23).

In addition to the pegmatitic occurrences, black schists were also mapped in this target area. These schists are intersected by quartz veins, which range from millimetric to decimetric scale and, a nearby boulder of pegmatite was also found, exhibiting bands of black schist (Fig. 5.24). The presence of quartz veining and the associated pegmatite contact suggest structural preparation of the host rock, facilitating late-stage fluid intrusion and crystallization (Černý, 1991; London, 2008).

The observed lithological and structural relationships at Target IX, particularly the contact geometry and the crosscutting quartz veins in black schists, are consistent with field evidence from other targets in the Barroso-Alvão pegmatite field, reinforcing the model of fracture-controlled pegmatite emplacement in structurally favorable zones within metasedimentary sequences (Noronha, 1987; Ribeiro, 1998; Lima, 2000; Sant'Ovaia, 2000).

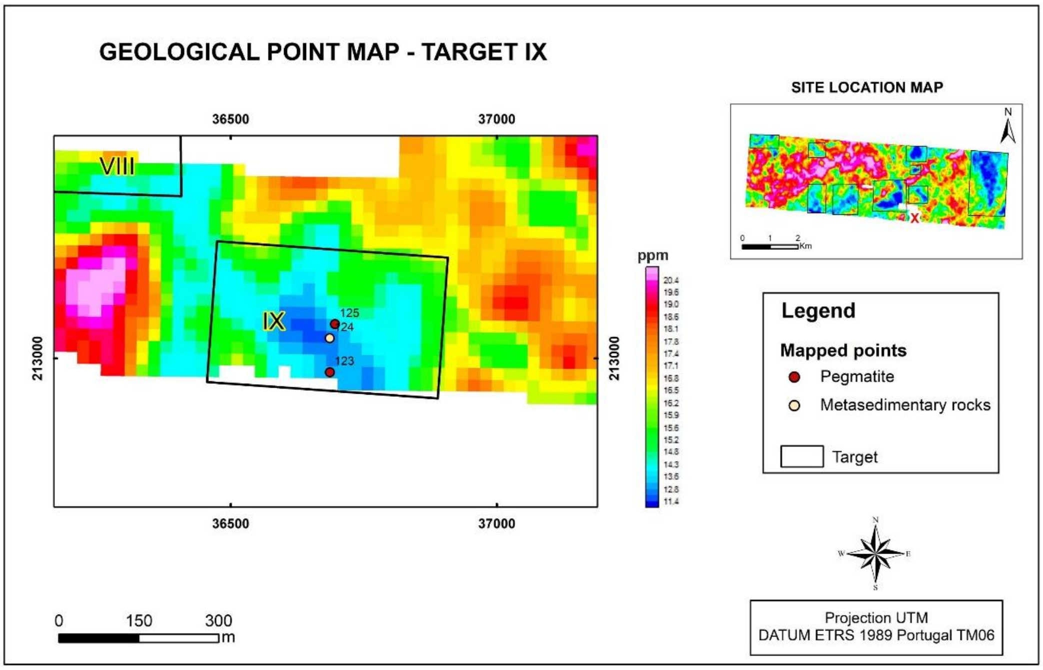

Fig 5.22: Geological point map focused on Research Target IX. Thorium (Th) concentration map provided by the GREENPEG project.

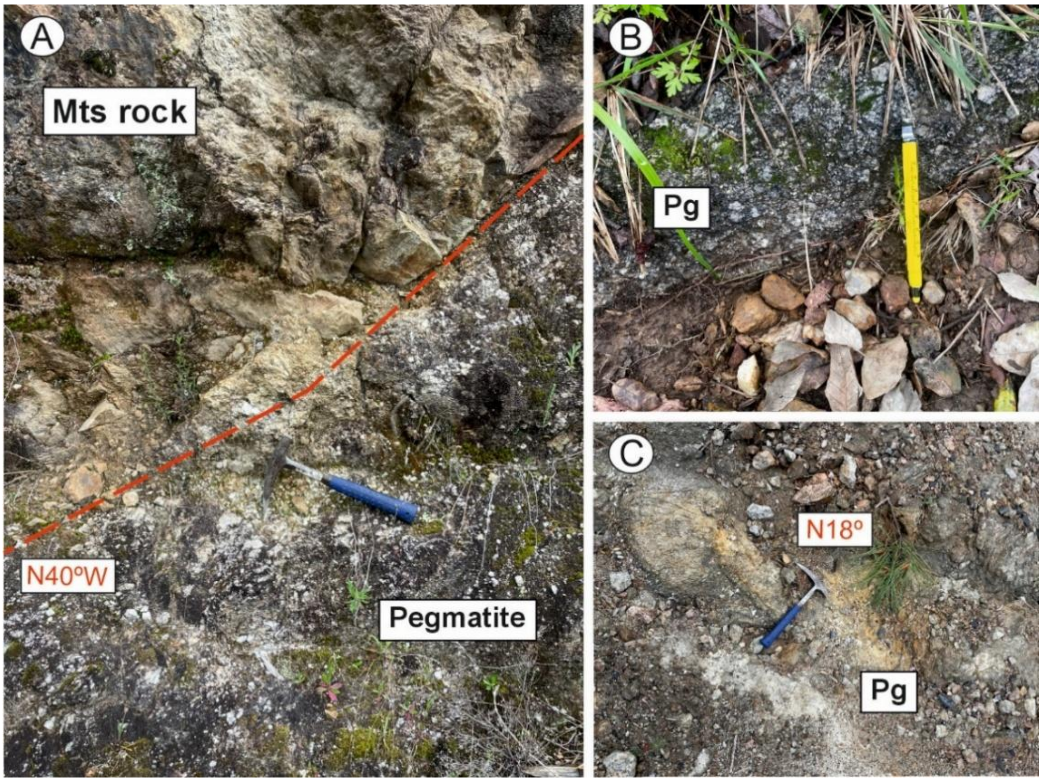

Fig 5.23: **A)** Contact between metasedimentary rock and pegmatite striking N40ºW (Point 123); **B)** Detail of the pegmatitic rock showing well-developed quartz and feldspar crystals (Point 125); **C)** Pegmatite outcrop striking N18º (Point 123). Mts = Metasedimentary; Pg = Pegmatite.

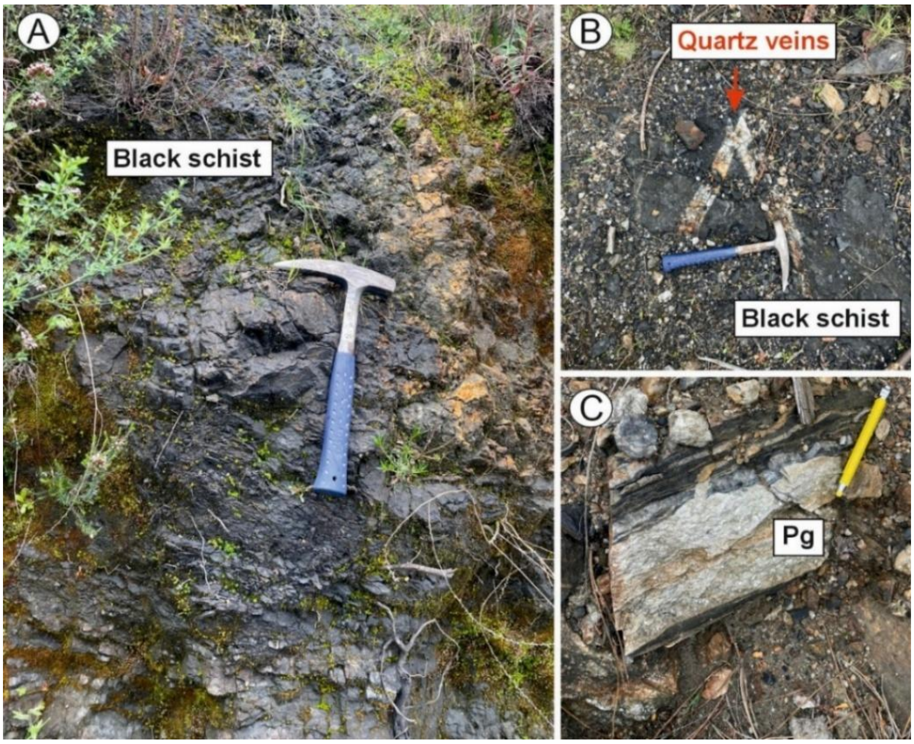

Fig 5.24: **A)** Outcrop of black schist. (Point 125); **B)** Black schist crosscut by a quartz vein (Point 125); **C)** Rolled block of pegmatite with bands of black schist (Point 125). Pg = Pegmatite.

5.2.10 Target X

Target X (Fig. 5.25) corresponds to the most extensive thorium anomaly identified within the study area. Field mapping revealed several well-exposed and representative pegmatite outcrops associated with this target, allowing for detailed structural, textural and mineralogical observations.

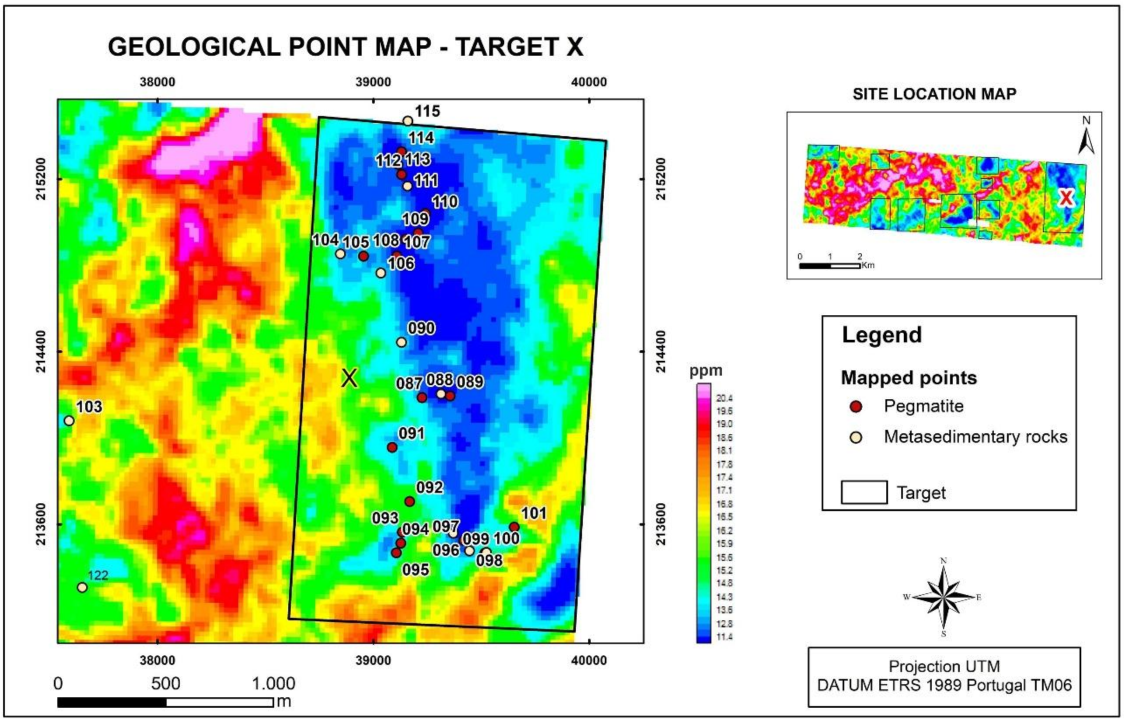

Fig 5.25: Geological point map focused on Research Target X. Thorium (Th) concentration map provided by the GREENPEG project.

The pegmatite bodies at this location are predominantly oriented in a N040° direction (Fig. 5.26), which is concordant with the regional structural trend, suggesting emplacement controlled by pre-existing foliation or fracture systems, likely resulting from the opening of spaces along the S_2 schistosity, produced during the third phase of Variscan deformation (D_3) (Lima, 2000). These bodies exhibit a characteristic pegmatitic texture, marked by coarse-grained mineral assemblages with prominent crystals of quartz and K-feldspar, a hallmark of slow crystallization from evolved melts rich in volatiles and incompatible elements (London, 2008).

Centimetre-scale quartz veins were also observed crosscutting the pegmatites, indicating the presence of late-stage fluid activity and possible reactivation of structures after the main crystallization phase. Additionally, a subtle but noticeable mineral alignment was observed within some pegmatite bodies, potentially reflecting magmatic flow structures or late deformational overprints (London, 2008).

The combination of structural alignment, coarse crystal habit, and late-stage veining supports the interpretation of Target X as an important pegmatitic corridor within the Barroso-Alvão field, strongly influenced by regional tectonic fabrics and late-Variscan structural reactivation (Dias & Ribeiro, 1995; Ribeiro, 1998; Noronha et al., 2006).

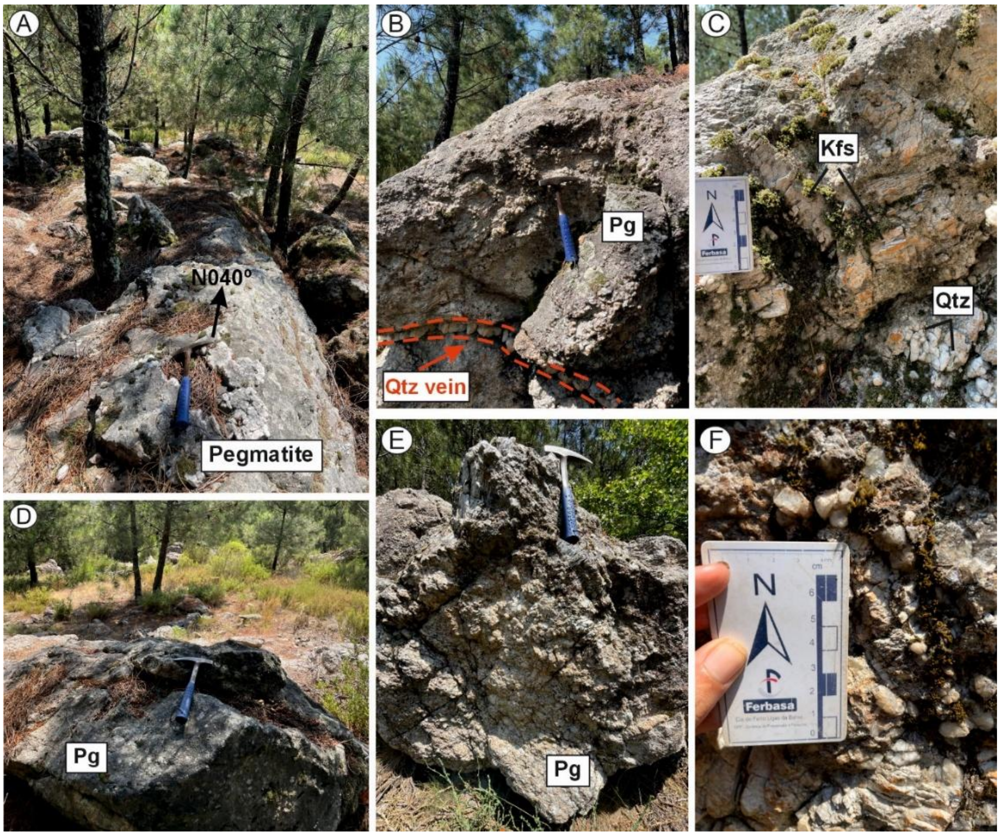

Fig 5.26: **A)** Pegmatite outcrop with N040° orientation (Point 93); **B)** Detail of quartz vein crosscutting the pegmatite (Point 94); **C)** Pegmatite with prominent quartz and K-feldspar crystals (Point 95); **D)** Pegmatite block (Point 94); **E)** Pegmatite outcrop with prominent quartz crystals (Point 91); **F)** Detail of centimeter-scale K-feldspar and quartz crystals (Point 91). Kfs = K-feldspar; Pg = Pegmatite; Qtz = Quartz.

The metasedimentary rocks mapped at Target X display well-developed deformational features, predominantly associated with the D_2 and D_3 phases of the Variscan Orogeny (Ribeiro, 1998). A prominent metamorphic differentiation is observed, characterized by alternating pelitic and psammitic layers, generating irregular banding that corresponds to the primary stratification (S_0) (Ribeiro, 1998; Lima, 2000).

Parallel to this metamorphic layering, the rocks are crosscut by quartz injections in the form of veins of various scales. These veins are themselves highly deformed, showing evidence of multiple deformation events, and highlight the strong ductile regime that affected these units during orogenesis.

The dominant foliation (S_2) measured across the outcrops shows a consistent orientation of approximately N030°, while minor crenulations, attributed to the D_3 phase, are present but not strongly developed.

A well-defined fold structure was recorded in the area, with an axial plane trending N056°/60°NW and a fold axis trending 5°→N114º, as illustrated in Fig. 5.27. These structural elements are consistent with late-Variscan, D_3, where the emplacement of pegmatite dykes may have occurred along the axial planes of the folds, potentially exploiting ruptures in S_2 and S_3 foliation planes (Ribeiro, 1998; Lima, 2000).

Another noteworthy aspect of this target is the significantly greater abundance of quartz, particularly when compared to the metasedimentary rocks observed in the targets located west of the Tâmega River. This feature may reflect enhanced silica mobility and veining related to localized deformation zones or metamorphic fluid activity during Variscan tectonometamorphism.

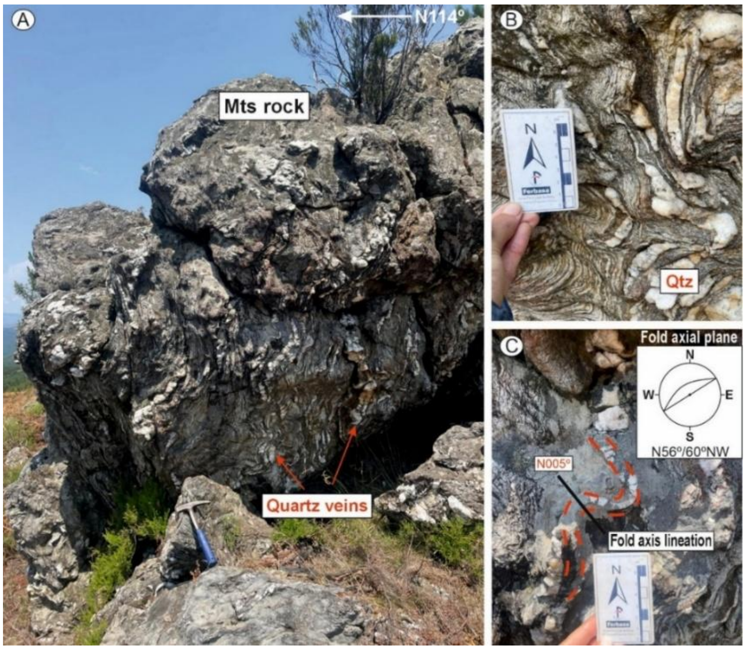

Fig 5.27: **A)** General view of strongly banded metasedimentary outcrop showing quartz-rich layers (Point 88); **B)** Detail of folded quartz and pelitic bands (Point 88); **C)** Fold axis lineation and axial plane orientation, consistent with late Variscan D3 folding (axial plane: N056°/60°NW; fold axis: 5°→ N114º) (Point 88). Mts = Metasedimentary; Qtz = Quartz.

An important structural and mineralogical feature within the area of Target X is the presence of the Adagoi Pegmatite Dyke, which has been extensively studied by several authors due to its mineralogical diversity and economic relevance (Noronha, 1987; Lima, 2000; Martins, 2009; Dias, 2011). This dyke supports the interpretation of the strong negative thorium (Th) anomaly in the area as being genetically associated with pegmatitic bodies.

The general orientation of the Adagoi dyke is N020° (Fig. 5.28), which is consistent with the structural trend observed in several of the pegmatite outcrops mapped within Target X. This concordance reinforces the hypothesis that pegmatite emplacement in the area was controlled by regional NNE-SSW trending structures developed or reactivated during the Variscan orogeny (Dias & Ribeiro, 1995; Lima, 2000).

According to investigations carried out by the Portuguese Geological Survey (IGM), including exploratory drilling campaigns, the Adagoi area contains multiple subparallel pegmatite dykes, several of which are mineralized in spodumene and petalite, key lithium-bearing minerals (Dias, 2011). The pegmatites in this sector are generally well-preserved, showing limited weathering and abundant outcrops. Their mineralogical assemblage includes feldspars, quartz, muscovite, spodumene, and petalite, with occasional occurrences of cookeite, a green lithium-rich chlorite-group mineral.

The mineralogical and structural features of the Adagoi dyke, particularly it's orientation and Th depletion, are directly comparable to those observed in the broader Target X anomaly. This reinforces the interpretation that the Th anomaly is not merely a reflection of lithological variation but is instead a robust geophysical indicator of subsurface pegmatite continuity, that could potentially be enriched in lithium minerals.

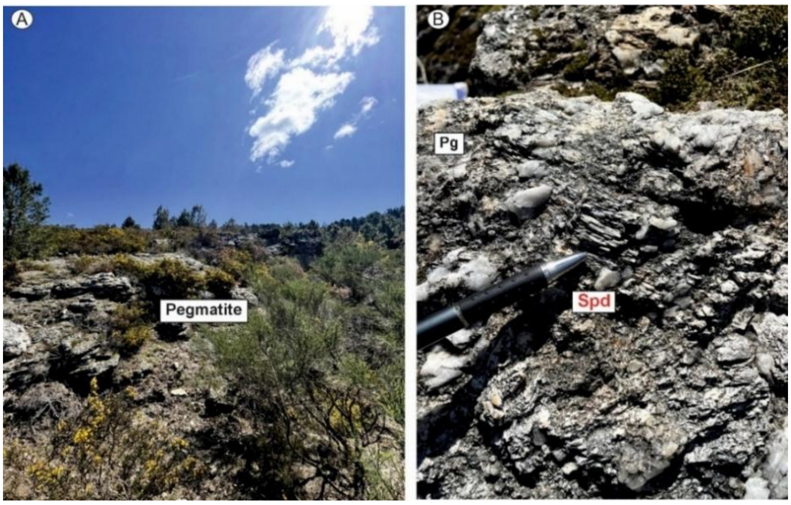

Fig 5.28: **A)** Overview of a pegmatite outcrop from the Adagoi dyke, showing a N020º orientation. **B)** Close-up of spodumene mineralization. Photographs taken during fieldwork activities of the Cartography and Field Geology course. Pg = Pegmatite; Spd = Spodumene.

5.2.11 Outcrops Outside the Main Research Targets

In addition to the ten main research targets, six supplementary outcrop points were mapped outside the primary anomalous zones, serving as control locations to assess the consistency of the geophysical interpretation and the potential lateral continuity of pegmatitic bodies (Fig. 5.29). Among these, Points 121, 126, and 127 are still located within the broader blue anomaly zone observed in the thorium (Th) concentration map, and all three correspond to pegmatite outcrops. In contrast, points 103 and 122 were identified as exposures of the metasedimentary host rock, with no evidence of pegmatitic material. At Point 102, a highly altered and friable pegmatite body was observed in direct contact with the surrounding metasediments.

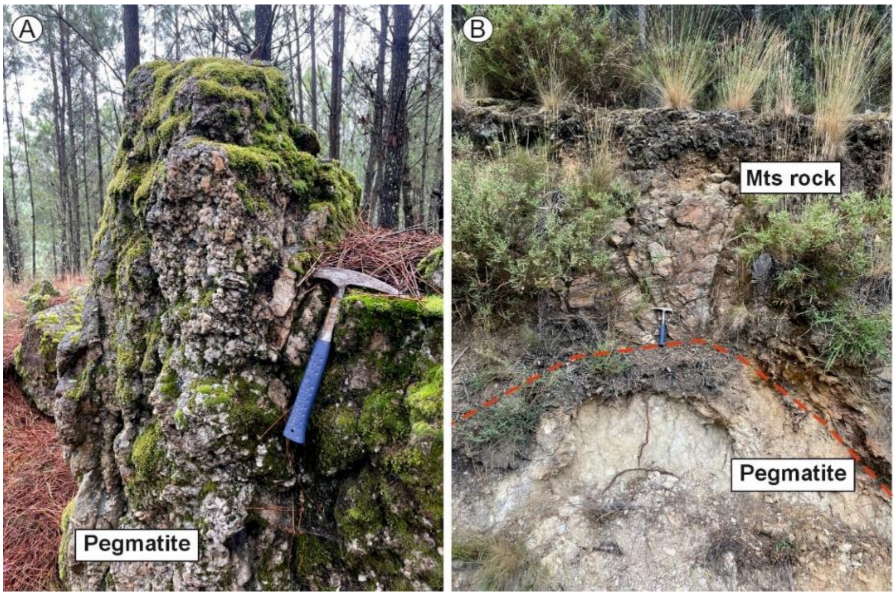

Fig 5.29 : **A)** Pegmatite block (Point 127). **B)** Contact between friable pegmatite and metasedimentary rock (Point 102). Mts = Metasedimentary

Chapter VI

Final Considerations

The results obtained in this study demonstrate that airborne gamma-ray spectrometry, particularly through the interpretation of negative thorium (Th) anomalies, can be validated as an effective method for the identification of pegmatite bodies. Field validation confirmed the presence of numerous pegmatite outcrops within zones previously defined as negative anomalies, including both newly recognized occurrences and pegmatitic bodies already described in the literature. These findings support the hypothesis that Th depletion, due to the geochemical characteristics of LCT-type pegmatites, constitutes a reliable geophysical indicator in radiometric surveys.

In addition to pegmatitic occurrences, metasedimentary host rocks were consistently found to contain quartz in the form of veins and segregations of variable scale. This recurrent association with silica may influence the radiometric signal, particularly in areas where pegmatites are not exposed or are absent at the surface. This factor becomes especially relevant along the eastern margin of the Tâmega River. Another noteworthy aspect of this target is the significantly greater abundance of quartz, particularly when compared to the metasedimentary rocks observed in the targets located west of the river. This feature may reflect enhanced silica mobility and veining related to localized deformation zones or metamorphic fluid activity during Variscan tectonometamorphism. As such, these quartz-rich lithologies could partially account for anomalous radiometric signatures, potentially masking or mimicking the geophysical response typically associated with pegmatites.

While this study focused on negative thorium anomalies, future work should include a systematic evaluation of positive Th anomalies as well. This would allow for a more refined discrimination between lithologies and geochemical processes, contributing to a broader understanding of radiometric variability in pegmatite-bearing terrains.

Finally, the newly identified pegmatite outcrops observed during fieldwork warrant further investigation, particularly regarding their potential for lithium mineralization. Detailed geochemical, petrographic, and mineralogical analyses are recommended to assess their economic relevance and to better classify these bodies within the LCT pegmatite spectrum.

References

Barros, R. (2017). Petrogenesis of the Leinster LCT (Li Cs Ta) pegmatite belt in southeast Ireland (PhD Thesis). School of Earth Sciences, University College Dublin.

Barros, R., Kaeter, D., Menuge, J. F., Fegan, T., & Harrop, J. (2022). Rare element enrichment in lithium pegmatite exomorphic halos and implications for exploration: Evidence from the Leinster albite-spodumene pegmatite belt, southeast Ireland. Minerals, 12(981).

Bertoldo, A. L., Alkmim, F. F., & Trouw, R. A. (1993). O comportamento estrutural das coberturas meso-neoproterozóicas do Cráton do São Francisco nas Serras do Espinhaço Setentrional, Central e Palmas de Monte Alto (MG-BA). In Anais do II Simpósio sobre o Cráton do São Francisco (pp. 205-207). SBG/NBA-SE.

Bradley, D. C., McCauley, A. D., & Stillings, L. L. (2017). Mineral-deposit model for lithium-cesium-tantalum pegmatites. US Geological Survey.

Cerný, P., & Ercit, T. S. (2005). The classification of granitic pegmatites revisited. The Canadian Mineralogist, 43, 2005-2026.

Carta Geológica de Portugal. (1998). Folha 6C - Cabeceiras de Basto, escala 1:50.000. Serviços Geológicos de Portugal/Instituto Geológico e Mineiro.

Carta Geológica de Portugal. (1998). Folha 6D - Vila Pouca de Aguiar, escala 1:50.000. Serviços Geológicos de Portugal/Instituto Geológico e Mineiro.

Černý, P., Chapman, R., Teertstra, D. K., & Novák, M. (2003). Rubidium- and cesium-dominant micas in granitic pegmatites. American Mineralogist, 88 (11-12), 1832-1835.

Černý, P., Harlov, D. E., & Austrheim, H. (2012). Granitic pegmatites as reflections of their sources. In D. E. Harlov & H. Austrheim (Eds.), Metasomatism and the chemical transformation of rock (pp. 297-341). Springer.

Černý, P. (1991a). Rare-element granitic pegmatites. Part I: Anatomy and internal evolution of pegmatite deposits. Geoscience Canada, 18, 49-67.

Černý, P. (1991b). Rare-element granitic pegmatites. Part II: Regional to global environments and petrogenesis. Geoscience Canada, 18, 68-81.

Cónego Júnior, D. (2019). Interpretação geofísica do Batólito de Catolé do Rocha PB-RN, Brasil (Dissertação de Mestrado). Universidade Federal de Pernambuco - UFPE.

Dantas, L. F. (2023). Identificação e caracterização dos pegmatitos litiníferos na região do Seridó, entre os Estados da Paraíba e do Rio Grande do Norte (Dissertação de Mestrado). Universidade Federal de Campina Grande.

Dias, R., & Ribeiro, A. (1995). The Ibero-Armorican Arc: A collision effect against an irregular continent? Tectonophysics, 246, 113-128.

Dias, F. C. L. (2016). Lithium mineralizations of Barroso-Alvão aplite-pegmatite field (Master's thesis). Departamento de Geociências, Ambiente e Ordenamento do Território, Universidade do Porto.

Errandonea-Martin, J., Garate-Olave, I., Roda-Robles, E., et al. (2022). Metasomatic effect of Li-bearing aplite-pegmatites on psammitic and pelitic metasediments: Geochemical constraints on critical raw material exploration at the Fregeneda-Almendra pegmatite field (Spain and Portugal). Ore Geology Reviews, 150, 105155.

Farias, P., Gallasteui, G., Lodeiro, F. G., Marquinez, J., Parra, L. M. M., & Catalán, J. R. M. (1997). Insights on the lithostratigraphy and structure of Central Galicia. Geology & Geophysics, 17(2), 51-62.

Froede, A. S. (2017). Análise geofísica do potencial pegmatítico na região de Ataléia (MG) (Monografia de TCC). Universidade Federal de Ouro Preto.

Iza, E. R. H. F., Horbe, A. M. C., Castro, C. C., & Herrera, I. L. I. E. (2018). Integration of geochemical and geophysical data to characterize and map lateritic regolith: An example in the Brazilian Amazon. Geochemistry, Geophysics, Geosystems, 19, 3254-3271.

Julivert, M., Fontboté, J. M., Ribeiro, A., & Conde, L. (1974). Mapa Tectónico de la Península Ibérica y Baleares. Instituto Geológico y Minero de España.

Kaeter, D., Barros, R., & Menuge, J. F. (2021). Metasomatic high field strength element, tin, and base metal enrichment processes in lithium pegmatites from southeast Ireland. Economic Geology, 116(1), 169-198.

Kaeter, D., Barros, R., Menuge, J. F., & Chew, D. M. (2018). The magmatic-hydrothermal transition in rare-element pegmatites from southeast Ireland: LA-ICP-MS chemical mapping of muscovite and columbite-tantalite. Geochimica et Cosmochimica Acta, 240, 98-130.

Kearey, P., Brooks, M., & Hill, I. (2009). Geofísica de exploração (M. C. M. Coelho, Trad.). São Paulo: Oficina de Textos.

Keyser, W., Müller, A., Steiner, R., Erambert, M., Kristoffersen, M., & Unterweissacher, T. (2023). Alpine eclogite facies modification of Li-Cs-Ta pegmatite from the Wolfsberg lithium deposit, Austria. Mineralium Deposita, 58, 1191-1210.

Lima, A. (2000). Estrutura, mineralogia e génese dos filões aplitopegmatíticos com espodumena da Região do Barroso-Alvão (Norte de Portugal) [PhD thesis, University of Porto and INPL, Nancy, France].

Lima, A., & Noronha, F. (2006). Da génese à aplicação tecnológica dos aplitopegmatitos litiníferos da Região do Barroso-Alvão e de Almendra. In VII Congresso Nacional de Geologia - Resumos alargados (Vol. 3, pp. 1183-1184). Universidade de Évora.

London, D. (2008). Pegmatites. Canadian Mineralogist Special Publication 10.

Lowrie, W. (2007). Fundamentals of geophysics (2nd ed.). Cambridge University Press.

Martins, T. (2009). Multidisciplinary study of pegmatites and associated Li and Sn-Nb-Ta mineralisation from the Barroso-Alvão region [PhD thesis, University of Porto].

Martins, T., Lima, A., Vieira, R., Noronha, F., & Dinis Machado, J. (2006). Aplitopegmatitos litiníferos, um exemplo de recursos geológicos no Município de Ribeira de Pena. In VII Congresso Nacional de Geologia - Resumos alargados (Vol. 3, pp. 1035-1036). Universidade de Évora.

Minty, B. R. S., Luyendyk, A. P. J., & Brodie, R. C. (n.d.). Calibration and data processing for airborne gamma-ray spectrometry. AGSO Journal of Australian Geology.

Müller, A., et al. (2025). The GREENPEG project toolset to explore for buried pegmatites hosting lithium, high-purity quartz, and other critical raw materials. Economic Geology, 120(3), 745-769.

Müller, A., Ihlen, P. M., & Kronz, A. (2008). Quartz chemistry in polygeneration Sveconorwegian pegmatites, Froland, Norway. European Journal of Mineralogy, 20, 447-463.

Müller, A., Spratt, J., Thomas, R., Williamson, B. J., & Seltmann, R. (2018). Alkali-F-rich albite zones in evolved NYF pegmatites: The product of melt-melt immiscibility. The Canadian Mineralogist, 56, 657-687.

Noronha, F. (1983). Estudo metalogénico da área tungstífera da Borralha [PhD thesis, University of Porto].

Noronha, F., Ramos, J. M. F., Rebelo, J., Ribeiro, A., & Ribeiro, M. L. (1981). Essai de corrélation des phases de déformation hercyniennes dans le NW de la P. I. Leid. Geol. Meded., 52(1), 87-91.

Noronha, F., Ribeiro, M. A., Almeida, A., Dória, A., Guedes, A., Lima, A., Martins, H. C., Sant’Ovaia, H., Nogueira, P., Martins, T., Ramos, R., & Vieira, R. (2006). Jazigos filonianos hidrotermais e aplitopegmatíticos espacialmente associados a granitos (Norte de Portugal). In Geologia de Portugal no Contexto da Ibéria (pp. 123-135). Universidade de Évora.

Quesada, C. (1991). Geological constraints on the Paleozoic tectonic evolution of tectono-stratigraphic terranes in the Iberian Massif. Tectonophysics, 185, 225-245.

Radley, D. C., et al. (2017). A preliminary deposit model for lithium-cesium-tantalum (LCT) pegmatites. US Geological Survey Professional Paper 1830.

Ribeiro, A., Antunes, M. T., Ferreira, M. P., Rocha, R. B., Soares, A. F., Zbyszewski, G., Almeida, F. M., Carvalho, D., & Monteiro, J. H. (1979). Introduction à la géologie générale du Portugal. Serviços Geológicos de Portugal.

Ribeiro, M. A., Martins, H. C., Almeida, A., & Noronha, F. (2000). Carta Geológica de Portugal, escala 1:50 000, 6-C (Cabeceiras de Basto), Notícia Explicativa. Serviços Geológicos de Portugal.

Ribeiro, M. A., Ramos, R., & Noronha, F. (2007). Pegmatite-aplite veins of Barroso-Alvão field: Lithostratigraphy and metamorphism of host rocks. In A. Lima & E. Roda-Robles (Eds.), Granitic Pegmatites: The state of the art - Fieldtrip guidebook (Memórias 9, pp. 39-45).

Ribeiro, M. A. (1998). Estudo litogeoquímico das formações metassedimentares encaixantes de mineralizações em Trás-os-Montes Ocidental: Implicações metalogénicas [PhD thesis, University of Porto].

Ribeiro, V. B., Mantovani, M. S. M., & Louro, V. H. A. (2013). Aerogamaespectrometria e suas aplicações no mapeamento geológico. Terra e Didática, 10, 29-51.

Sant'Ovaia, H. (2000). O maciço granítico pós-tectónico de Vila Pouca de Aguiar: Estudo petro-estrutural e mecanismo de instalação [Master's thesis, Université Paul Sabatier - Toulouse III & Universidade do Porto].

Sant'Ovaia, H., Ribeiro, M. A., Martins, H. C. B., & Noronha, F. (2011). Notícia explicativa da Carta geológica de Portugal na escala 1:50 000 - Folha 6D - Vila Pouca de Aguiar. LNEG - National Laboratory of Energy and Geology.

Schön, J. H. (2015). Nuclear/Radioactive Properties. In Developments in Petroleum Science, VOL. 65.

Shives, R. B. K., Charnonneau, B. W., & Ford, K. L. (2000). The detection of potassic alteration by gamma-ray spectrometry - Recognition of alteration related to mineralization. Geophysics, 65, 2001-2011.

Simmons, W. B., & Webber, K. L. (2008). Pegmatite genesis: State of the art. European Journal of Mineralogy, 20(4), 421-438.

Simmons, W. (2007). Pegmatite genesis: Recent advances and areas for future research. In Granitic Pegmatites: The State of the Art - International Symposium. Porto, Portugal.

Telford, W. M. W., Geldart, L. P., & Sheriff, R. E. (1990). Applied geophysics. Cambridge University Press.

Wise, M. A., et al. (2022). The mineralogical-geochemical classification of granitic pegmatites. Minerals, 12, 1002.

Wise, M., Müller, A., & Simmons, W. (2022). A proposed new mineralogical classification system for granitic pegmatites. The Canadian Mineralogist, 60, 229-248.

Websites Consulted

https://www.fc.up.pt/peg2007/

https://greenpeg.eu/

https://repositorio-aberto.up.pt/

https://www.researchgate.net/

Software Used

ArcGIS, version 10.8

Google Earth 2025

Applications Used

Avenza Maps